TOWARD MURA CHARACTERIZATION AND DAHPS INHIBITOR DESIGN

CHARACTERIZATION OF FOSFOMYCIN-RESISTANT MURA FROM BORRELIA BURGDORFERI, FRAGMENT-BASED INHIBITOR DESIGN FOR AROA AND DAHP SYNTHASE

By

SHAN JIANG, B. Sc.

A Thesis

Submitted to the School of Graudate Studies

In Partial Fulfillment of the Requirements

For the Degree

Master of Science

McMaster University

MASTER OF SCIENCE (2011) McMaster University

(Chemical Biology Graduate Program) Hamilton, Ontario

TITLE: Characterization of Fosfomycin-Resistant MurA from *Borrelia burgdorferi*, Fragment-based Inhibitor Design for AroA and DAHP Synthase

AUTHOR: Shan Jiang, B. Sc. (Peking University, Beijing, P.R. China)

SUPERVISOR: Dr. Paul J. Berti

NUMBER OF PAGES: xi, 74

Abstract

MurA catalyzes the first committed step of peptidoglycan biosynthesis and it is the target of the antibiotic fosfomycin. Due to a Cys-to-Asp substitution in the active site, MurAs from a number of pathogenic bacteria, including *Mycobacterium tuberculosis* and *Borrelia burgdorferi* (Lyme disease), are fosfomycin resistant. His-tagged *Borrelia burgdorferi* MurA (Bb_MurA) and its D116C mutant have been successfully expressed, purified and characterized. The k_{cat} value of wild-type Bb_MurA was 0.74 ± 0.01 s^{-1}. The D116C mutant's k_{cat} decreased by 25-fold and was fosfomycin sensitive. The pH profiles of k_{cat} for both Bb_MurA and its mutant were characterized. There was little difference in pK_{a1} values, but the pK_{a2} value shifted from 7.4 ± 0.2 in wild-type enzyme to a value >11 in the mutant. This demonstrated that the pK_{a2} of 7.4 was due to D116, and that it must be protonated for activity. Fosfomycin inactivation of Bb_MurA$_{H6}$ (D116C) was time-dependent and only proceeded in the presence of UDP-GlcNAc. The dissociation constant, K_i, was 5.7 ± 0.4 μM and rate of covalent modification, k_{inact}, was 0.021 ± 0.003 s^{-1}.

DAHP synthase catalyzes the first committed step in the shikimate pathway, and its catalysis has been proposed to proceed through two oxacarbenium ion intermediates. Pyruvate oxime, glyoxylate oxime and 4-imidazolecarboxylic acid have been evaluated as inhibitors of DAHP synthase. In the presence of glycerol 3-phosphate, the fitted K_i values of pyruvate oxime and glyoxylate oxime were 7.6 (± 0.9) × 10^{-5} M and 7.4 (± 1.7) ×

10^{-5} M, respectively. 4-Imidazolecarboxylic acid's inhibition was cooperative, and its binding was competitive with respect to PEP, and uncompetitive with respect to E4P. Its equilibrium dissociation constant was 3.0 (± 0.2) × 10^{-3} M.

Acknowledgements

I would like to take this opportunity to thank my supervisor Dr. Paul Berti for giving me this invaluable experience of studying at McMaster University and working on this project. I greatly appreciate all the guidance, instruction and encouragement you provided me. I would like to thank my committee members, Dr. Giuseppe Melacini and Dr. Murray Junop, for the insightful feedbacks and suggestions you provided me during my committee meetings.

I would like to thank the Berti lab members, Naresh Balachandran, Vincent Azhikannickal, Vladimir Popovic, Jason Thomas, Vamana Rajeswaran, Lauren Wilson, Xiaoyi Ji, Peter Kim, Jenny Zheng and Adam Mopham. It has been my great honor to work in such a supportive lab, and thank you for making my time in the lab into a pleasant and encouraging experience.

Finally, I want to thank my parents, who provide me endless love and support even though they are away in China. I would not be able to accomplish anything without your encouragement. Thank you for always being so supportive and selfless to me through my life.

Table of Contents

List of Abbreviations

MurA:	enolpyruvyl UDP-GlcNAc transferase
AroA:	enolpyruvyl shikimate 3-phosphate synthase
PEP:	phosphoenolpruvate
UDP-GlcNAc	UDP-*N*-acetylglucosamine
S3P:	shikimate 3-phosphate
ddS3P:	4.5-dideoxyshimikate 3-phosphate
DAHPS:	3-deoxy-*D*-arabino-heptulosonate 7-phosphate synthase
THI:	tetrahedral intermediate
EPSP:	5-enolpyruvyl shikimate 3-phosphate
E4P:	erythrose 4-phosphate
KDO8PS:	3-deoxy-*D*-manno-2-octulosonate 8-phosphate
A5P:	*D*-arabinose 5-phosphate
Bb_MurA:	*Borrelia burgdorferi* MurA
Ec_MurA:	*Escherichia coli* MurA
Ec_AroA:	*Escherichia coli* AroA
MG/AM:	Malachite Green / ammonium molybdate
Pi:	inorganic phosphate
TS:	transition state
IPTG:	isopropyl-β-*D*-thiogalactopyranoside
PMSF:	phenylmethylsolfonyl fluoride

List of Figures

List of Tables

Introduction

The discovery of antibiotics symbolized the epic victory for human beings in the struggle against infectious diseases and pathogenic bacteria. However, we are currently facing a severe health-threatening situation, due to the bacterial evolution of antibiotic resistance, and the slow progress in the development of new antibiotics. Pan-resistant bacteria emerged in clinical settings and they are resistant to all known antibiotics. Most of the antibiotics in use today were discovered in the 1940s and 1950s, and only two classes of new antibiotics were tested to be effective and approved for clinical use since the 1960s[1].

Enzymes are important targets for antibiotic development. Enzymes present the restricted geometry and unique hydrophobic environment for challenging chemical reactions, and they provide rate enhancement by a factor up to 10^{21}-fold comparing to non-enzymatic reactions[2]. The enzyme inhibitors typically resemble the chemical and electrostatic features of the substrates, intermediates, or the transition-state (TS) structures in the catalytic reactions[3]. The majority of the enzyme-targeted drugs in the market are derived from the substrate structures[3], but the design of transition-state inhibitors has become more prevalent recently due to their high affinity to the target enzymes.

The enzyme of interest MurA, its homologous enzyme AroA

Enolpyruvyl UDP-GlcNAc transferase (MurA) and enolpyruvyl shikimate 3-phosphate synthase (AroA) are the only two known carboxyvinyl transferases. MurA catalyzes the first committed step in the biosynthesis of peptidoglycan, which is an essential component of the bacterial cell wall[4]. AroA catalyzes the sixth step in the shikimate pathway, which provides the bacteria with essential aromatic amino acids, vitamin K, ubiquinone and enterochelin[5]. In both catalysis reactions, an enolpyruvyl moiety is transferred from phosphoenolpyruvate (PEP) to the C3 hydroxyl of the sugar substrate, with an inorganic phosphate released[6,7] (Figure 1). Catalysis proceeds through an addition-elimination mechanism, forming a non-covalent tetrahedral intermediate (THI)[6].

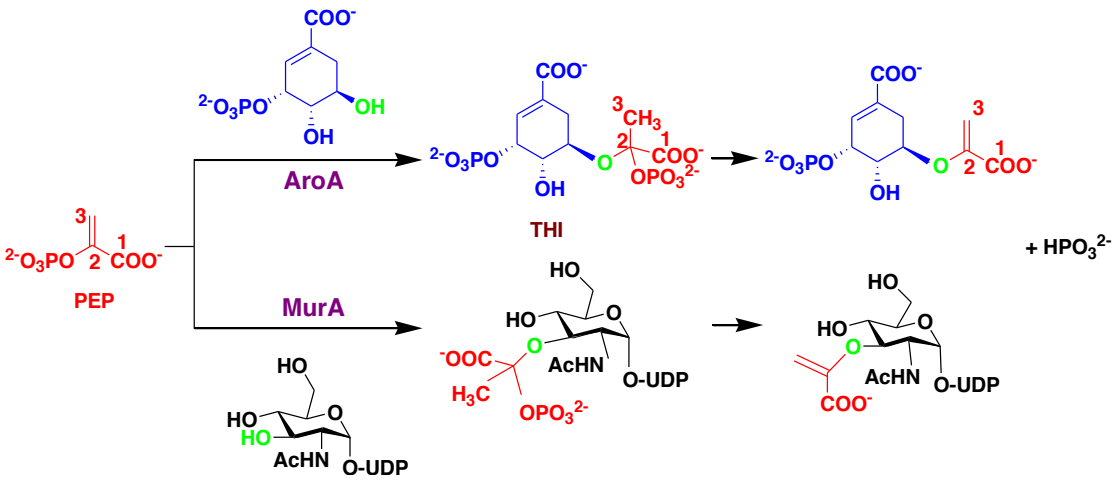

Figure 1. MurA and AroA's catalytic reactions. (Figure courtesy of Dr. Paul Berti)

Good targets for antimicrobial development

Peptidoglycan is a crosslinked carbohydrate polymer, which provides bacterial cells with mechanical resistance to the osmotic pressure fluctuations and maintains the

defined cell shape[8]. Peptidoglycan biosynthesis consists two complex stages. The first stage occurs in the cytoplasm, and is catalyzed by a series of enzymes, MurA-MurF. Interference to the biosynthesis and assembly of peptidoglycan leads to the death of bacterial cells. This pathway is only present in prokaryotic cells[8], making all the enzymes involved, including MurA, attractive targets for antibiotics development. MurA is conserved across both Gram positive and Gram negative bacteria and has no mammalian homolog[4].

Bacteria, parasites and plants require the shikimate pathway for the synthesis of tyrosine, phenylalanine and tryptophan. Mammals, lacking this pathway, can only obtain these amino acids from their diet[5]. Deletion of the enzymes involved in shikimate pathway is lethal by making bacteria auxotrophs for the aromatic amino acids. AroA deficient bacteria are avirulent and used as vaccines. Detailed understanding about the catalytic mechanisms of DAHP synthase and AroA, the first and sixth enzymes in the shikimate pathway, will provide a rational approach for inhibitor design.

X-ray crystal structures of MurA and AroA

More than 30 crystal structures have been solved for MurA and AroA[7-10]. These two homologous enzymes share essential structural similarities, even they have only 18% sequence identity[11]. Both enzymes are single polypeptide chains containing two globular domains, hinged by a double-stranded linker[8, 12]. The two domains share a similar main-chain fold, with three parallel internal helices surrounded by three helices and three

four-stranded β-sheets, known as "inside-out α/β barrel" (Figure 2). The catalytic site is located in a deep cavity at the interface of the two domains[10]. The substrate-free enzymes maintain the open-state structure. Upon substrate binding, both enzymes undergo a conformational change between open and closed states, characterized by the two domains approaching each other[9, 10]. MurA has a ten-residue active site loop, P112 to P121. The loop is solvent accessible in the open conformation, and it closes like a flap over the active site upon ligand binding. The sequence of the loop is highly conserved, except for two Ala residues and a Cys-to-Asp substitution in a number of pathogenic bacteria.

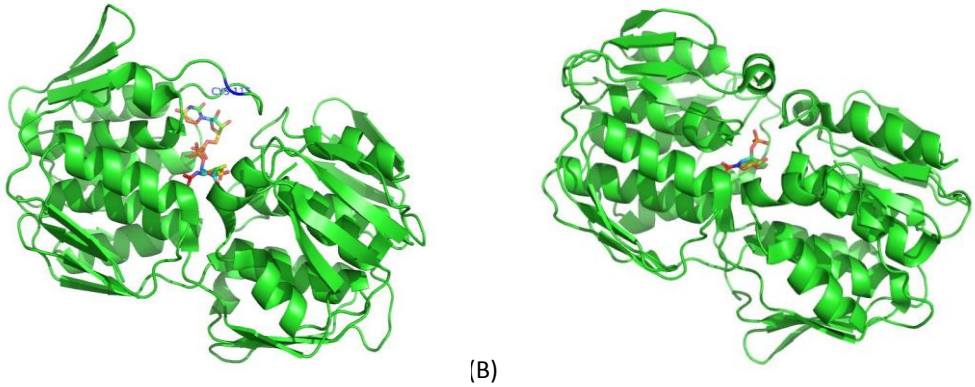

(A) (B)

Figure 2. (A) *E. coli* MurA in complex with substrate UDP-GlcNAc[6]. (B) *E. coli* AroA in complex with substrate S3P[13].

MurA and AroA's mechanisms

Extensive studies have been done to explore the mechanism MurA and AroA share in catalysis. In MurA's reaction, the binding of UDP-GlcNAc introduces a conformational change of MurA, which facilitates PEP's binding. AroA's catalysis has also been proposed

to follow an sequential mechanism, with shikimate 3-phosphate (S3P) binding first and followed by PEP[14, 15]. Gruys group showed later that the binding of substrates in AroA's reaction was random and synergistic[16]. Both the addition and elimination steps in the reaction pathways are subject to general acid/base catalysis[17]. In the addition step, the methylene group of PEP is protonated at C3 by the general acid catalyst, and attacked at C2 by the hydroxyl group from either UDP-GlcNAc or S3P. Then the general base catalyst deprotonates the C3 methyl group of THI, and inorganic phosphate is eliminated. The departure of phosphate is achieved through the unusual C-O bond cleavage[18].

The THI in both reactions have been trapped, purified and subjected to extensive mechanistic studies. The THIs are acid labile and relatively stable in basic environment. AroA's THI has a half-life of 15 min at pH 7, and it increases to > 2 weeks when the pH rises to above 12[19]. The non-enzymatic THI breakdown is general acid catalyzed, and the rate is accelerated by 1.5×10^5-fold in presence of AroA. Under pre-steady state conditions, AroA's THI is formed and degraded fast enough to account for the observed turnover rate, thus it is kinetically competent and identified as a true intermediate in catalysis[11]. AroA's catalysis is fully reversible, with equilibrium favoring the forward direction to EPSP + Pi versus the reverse reaction to S3P + PEP by 15-fold [11].

MurA's THI exhibits slow-binding pattern towards the enzyme. Once bound, the rate of breakdown is accelerated by 8×10^4-fold[6].

MurA's inhibitors

Despite the essential role MurA plays in the survival of bacterial cells, and thus the potential for development of novel antibacterial agents, the only established antibiotic that specifically targets this enzyme is fosfomycin, which was discovered in the 1960s[20]. Fosfomycin is a naturally occurring antibiotic, which alkylates the thiol group of the unusually nucleophilic Cys residue in susceptible enzymes[8] (Figure 3). The alkylation process is irreversible, and only proceeds in presence of UDP-GlcNAc[21].

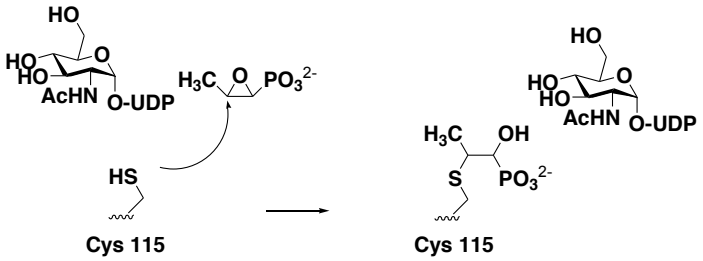

Figure 3. Fosfomycin alkylates the active site Cys residue in presence of UDP-GlcNAc.

Fosfomycin is able to treat urinary tract infections in a single dose, but its spectrum is limited by the requirement of active transport through the bacterial cell membrane, and by the fact that it only inhibits Cys-containing MurAs. The natively Asp-containing MurAs are intrinsically fosfomycin-resistant, including those from *Mycobacterium tuberculosis*, *Chlamydia trachomatis*, *C. pneumoniae*, *Treponema pallidum*, and *Borrelia burgdorferi* (Figure 4). *M. tuberculosis* has been a devastating pathogen of humans for centuries and it continues to cause 2 million deaths annually. In 2007, half a million cases of multi-drug-resistant tuberculosis infection were reported, accounting for up to 13% of newly diagnosed cases[1]. Lyme disease is an arthropod-

borne infection caused by the spirochete *B. burgdorferi*. It is a chronic multisystem disorder with symptoms that include skin rashes, arthritis, meningitis, optic neuritis, facial nerve palsy and atrioventricular nodal block. It is the most prevalent vector-borne disease in the United States and Europe[22].

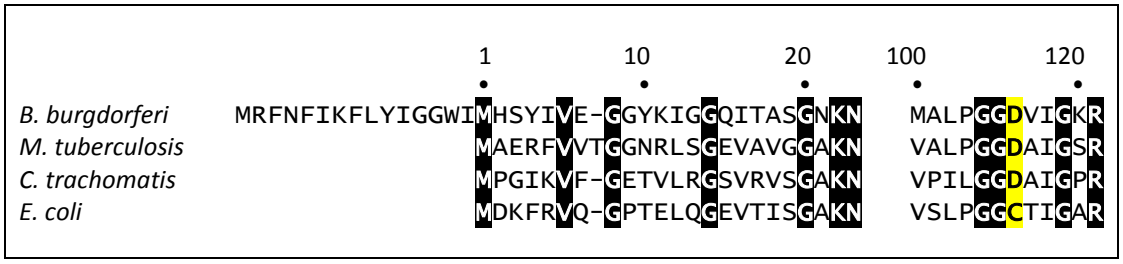

Figure 4. Amino acid sequences of *B. burgdorferi* MurA, other representative Asp-containing MurAs, and *E. coli* MurA.

A number of novel inhibitors for MurA have been reported, but none of them is as potent as fosfomycin with respect to their functionality or drug-like properties. Previous studies from our group have revealed that UDP-*N*-acetylmuramic acid (UDP-MurNAc), the product of the second enzyme in the peptidoglycan biosynthesis pathway, is a potent inhibitor to MurA[23]. The fact that significant amount of UDP-MurNAc was copurified with overexpressed recombinant MurA from *E. coli* suggests that UDP-MurNAc could act as a feedback inhibitor of MurA in regulating peptidoglycan biosynthesis in vivo. Natural products, such as the sesquiterpene lactone cnicin, tuliposides, and terreic acid, inhibit MurA in vitro, but have no inhibitory effect on bacterial cells[24]. Thus Schonbrunn's group hypothesized that the in vitro reactive compounds predominantly interact with proteins located on the outside surface of the

bacterial cell membrane without even entering the cytoplasm[24]. Only inhibitors with latent electrophilicity can selectively target MurA in vivo without unspecific interactions with other proteins. Feglymycin was recently discovered to be an specific inhibitor targeting MurA and MurC in the peptidoglycan biosynthesis pathway, but the inhibition was non-competitive to both substrates of either enzyme[25].

AroA's inhibitors

AroA's most potent inhibitor so far, the herbicide glyphosate (*N*-(phosphonomethyl)glycine), forms a tight ternary complex with the enzyme in the presence of S3P and competitively inhibits PEP binding with a K_i of 1.1 μM[26,27]. Glyphosate had been suggested to be a transition-state analogue mimicking a protonated carbenium ion species of PEP, but later evidence challenged this theory with the observations that: 1) glyphosate binding is uncompetitive with respect to EPSP[28], implying that it is not occupying the same physical space as the enolpyruvyl moiety; 2) The bisubstrate inhibitor (**2**, Figure 5), which structurally resembles the key features of S3P and PEP, is a potent inhibitor to AroA. In comparison, molecule **3**, which combines the structural features of S3P and glyphosate, is only a modest inhibitor, indicating that PEP and glyphosate are not superimposable in the active site[29]; 3) a TS inhibitor is expected to exhibit a correlation between the potency (K_i) of its analogous inhibitors and the catalytic efficiency (k_{cat}/K_M) of the corresponding substrates. Various AroA mutants have been characterized, but no enzyme demonstrates such correlation[29]. Thus glyphosate is assumed not as a TS mimic[29]. Even though it is effective as a herbicide,

glyphosate is not an antibiotic, presumably because it cannot penetrate the cell wall with its anionic phosphonate group.

Other inhibitors developed for AroA up to present could be divided into two categories: PEP analogues and THI analogues. To modify the structural scaffold of PEP, both carboxylate and the phosphate functional groups have been altered. Halogenation of the methylene group was explored[30], and the best inhibition originates from the ones containing modifications at the vinyl protons, such as (Z)-3-fluoro-PEP. AroA exhibits higher affinity towards the THI structure than its substrates[31], so several THI analogues have been synthesized and pursued. The (*R*)- and (*S*)- diastereomers (Figure 5) has been designed as phosphonate THI analogues and evaluated to be competitive inhibitors with K_i's against S3P of 16 nM and 750 nM and K_i's against EPSP of 15 nM and 1130 nM, respectively[31].

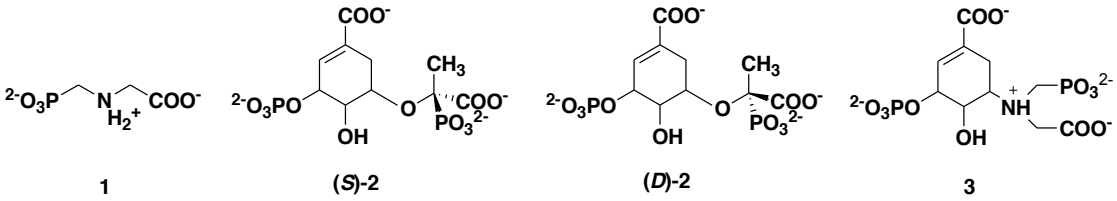

Figure 5. AroA's inhibitors.

Essential residues in MurA's catalysis

The C115 residue in MurA has been proposed to have two distinct roles in catalysis, one as a general acid/base catalyst[20], and another role in product release[32]. As these

proposed roles occur in different parts of the catalytic cycle, it is possible that both are correct.

The C115A and C115S mutants of *Escherichia coli* MurA (Ec_MurA) exhibited less than 0.05% of wild type activity, demonstrating the importance of C115 in catalysis[20]. The C115D mutant remained active, with a modest 10-fold decrease in $k_{cat}/K_{M,\ PEP}$[20]. In its proposed role as a general acid/base catalyst, the thiol of Cys or carboxylic acid of Asp protonates the double bond of PEP at C3, and may electrostatically stabilize the positive charge at C2 of the PEP cation. The thiolate or carboxylate form would then act as a general base in the elimination step by deprotonating the methyl group of THI[20] (Figure 6). Resistance of Asp-containing MurAs to fosfomycin is likely a consequence of the decreased nucleophilicity of carboxylates compared to thiolates. The pK_a value of Ec_MurA C115 was 8.3, which indicates that at physiological pH it is protonated and capable of donating a proton[33].

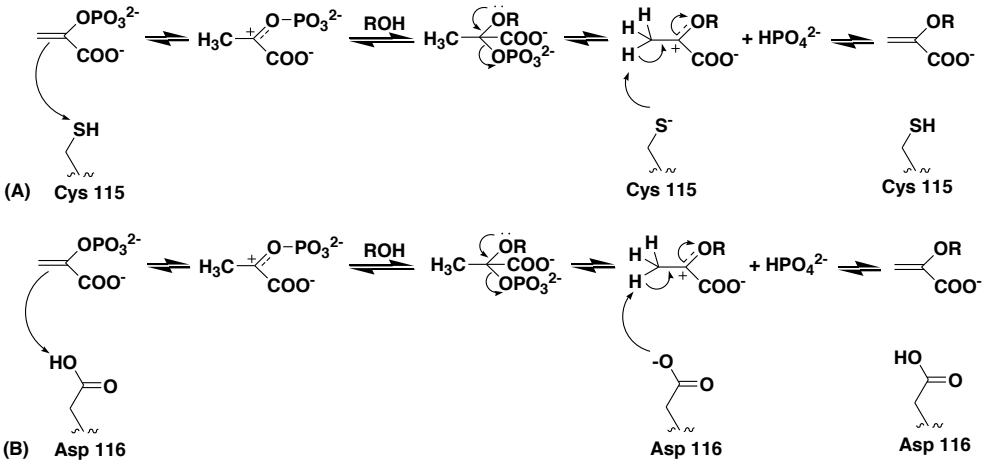

Figure 6. Cys115/Asp116 proposed role as general acid/base catalyst

C115 is also proposed to be involved in product release. As part of product release process, the enzyme conformation switches from the closed state back to the open state by passing through a “staged conformation”. Staged conformation is the structure the enzyme exhibits when the Pi product binds to the polyanion binding site, which is located in a tunnel between the active site and the protein surface[6]. Staged conformation possesses a unique set of protein-ligand and intramolecular side-chain interactions that are distinct from either the open or the closed phase of the enzyme. The R397 side chain in the staged conformation tracks Pi as it moves to the polyanion binding site, and the L370 side chain moves into the space vacated by R397 (Figure 7). The Ec_MurA C115S mutant was able to catalyze only a single turnover and was unable to form the "staged conformation" in order to release the product[20], evidence that C115 is required for product release. The Ec_MurA(C115D) mutant yields a high k_{cat} value[20], which demonstrates that the Asp side chain was still able to function in product release, and presumably would be capable of playing the same role in *B. burgdorferi* MurA (Bb_MurA).

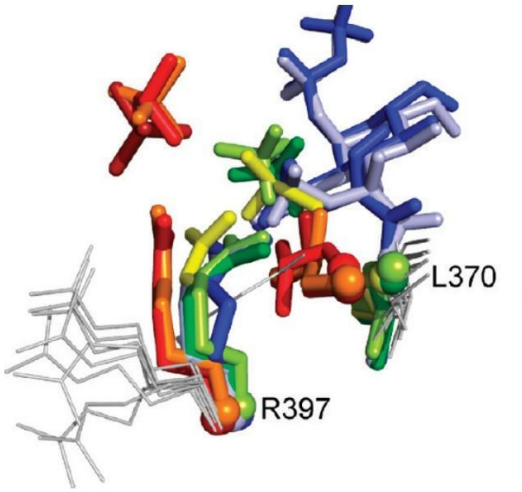

Figure 7. The R397 and L370 side chains in different conformations of enzyme. The "open conformation" is presented in gray color; "Staged conformation" is presented in red and orange color; The "closed conformation" is presented in yellow, green and blue color. (Figure from reference 7)

Essential amino acid residues in AroA's catalysis

AroA has been subjected to numerous mechanism studies, but the responsible residues in the catalysis remain in controversy. Figure 8 represents different mechanisms that have been proposed by research groups.

Using partitioning analysis and site-directed mutagenesis, previous studies from our group revealed that a large number of amino acid residues are directly involved in the catalysis, and the same residues promote the THI breakdown in both forward and reverse reactions[7]. Mizyed proposed that in the addition step, Lys22 functions as a general base and Glu341 as the general acid. Their roles are reversed in the elimination step, with Lys22 serving as general acid and Glu341 as general base[34]. In the paper published in 2009, we reported that D313 and E341 are the primary catalytic residues, and K22's greatest contribution is for substrate binding, even it might also be involved in

general acid/base catalysis. This is consistent with E341's proposed role as an acid/base catalyst. In addition, E341 and D313 are discovered to form an "electrostatic sandwich" to stabilize the cationic intermediates in THI formation and breakdown[7].

(A) Mizyed et al. Mechanism[34,7]

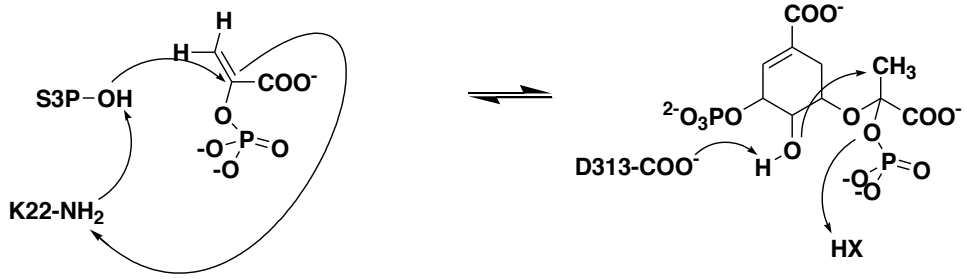

(B) Eschenburg et al. Mechanism[12]

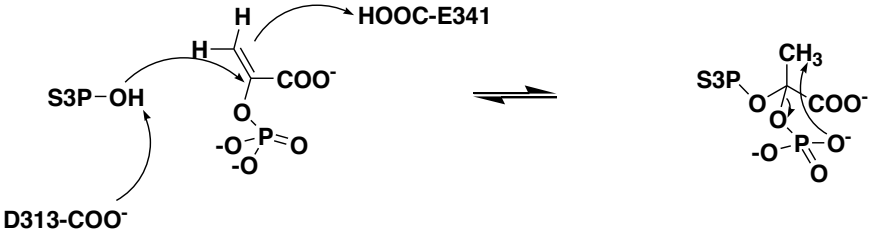

(C) An et al. Mechanism[54]

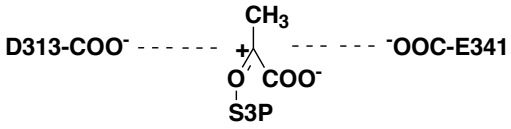

(D) Electrostatic sandwich of EPSP cation[7]

Figure 8. Proposed mechanisms of AroA's catalysis.

Fragment-based drug discovery approach

As the most prevalent tool utilized in pharmaceutical companies, high-throughput screening (HTS) achieved a fundamental revolution by taking advantages in automation, miniaturization, increased assay speed and sensitivity[35]. Using combinatorial libraries, a well-established HTS assay is capable of screening 100,000 compounds in a single day[36]. However, a significant proportion of the primarily identified hits lost their drug-like properties during the optimization process[37]. This dilemma gives rise to the urgent need for new drug discovery methods, in which creating more valid chemical structures is more emphasized.

In the early 1980s, Jencks first demonstrated that the combinations of molecular fragments could be used to explore high affinity inhibitors towards the target enzyme[38]. The fragments used in this approach are designed and selected based on well-defined protein-ligand interaction and protein structural information. The chemical and electrostatic characteristics allow greater possibility for the molecules to find the complementary binding-site on the target protein, so the binding efficiency and specificity are achieved. A screening library in fragment-based approach typically contains less than 1000 molecules, most of which are synthetically accessible and water soluble[39]. The definition of a fragment varies, but its molecular weight and lipophilicity (cLogP) are usually in the range of 120-250 Da and 1-3 unit, respectively. They are lower than drug-like compounds[39], allowing further optimization for the screened compound to possess the drug-like properties after being identified as a lead. The paramount

advantage of this method originates from the reciprocal relationship between the fragment's complexity and the protein binding site, which affords insightful understanding of protein structural and catalytic information for the subsequent optimization of the primary lead.

Transition state theory and analog design

In the reaction coordinate, transition state is a distinct species whose formation requires the highest energy investment. Enzymes accelerate the reaction rate by lowering the activation energy for the transition state (Figure 9). The highly unstable transition state structure exists for approximately 10^{-13} second, which resembles the conversion time of a bond from the vibrational mode to the translational mode[40]. Forming the transition state requires the greatest activation energy and is directly proportioned to the enhancement of catalytic rate. The dissociation constants for the substrates are usually in the range of 10^{-3}-10^{-6} M, while the transition state molecules possess binding affinity in the range of 10^{-14}-10^{-23} M[40]. Molecules which are transition state analogues, and capture all the essential chemical and electrostatic features of the transition state structures should bind tightly to the target enzymes. Enzymes are less likely to evolve resistance to transition state inhibitors, because if they mutate to decrease their affinity to the TS inhibitors, they will lose the affinity to their natural substrates simultaneously. Thus the TS mimics have become one of the major trends for inhibitor development.

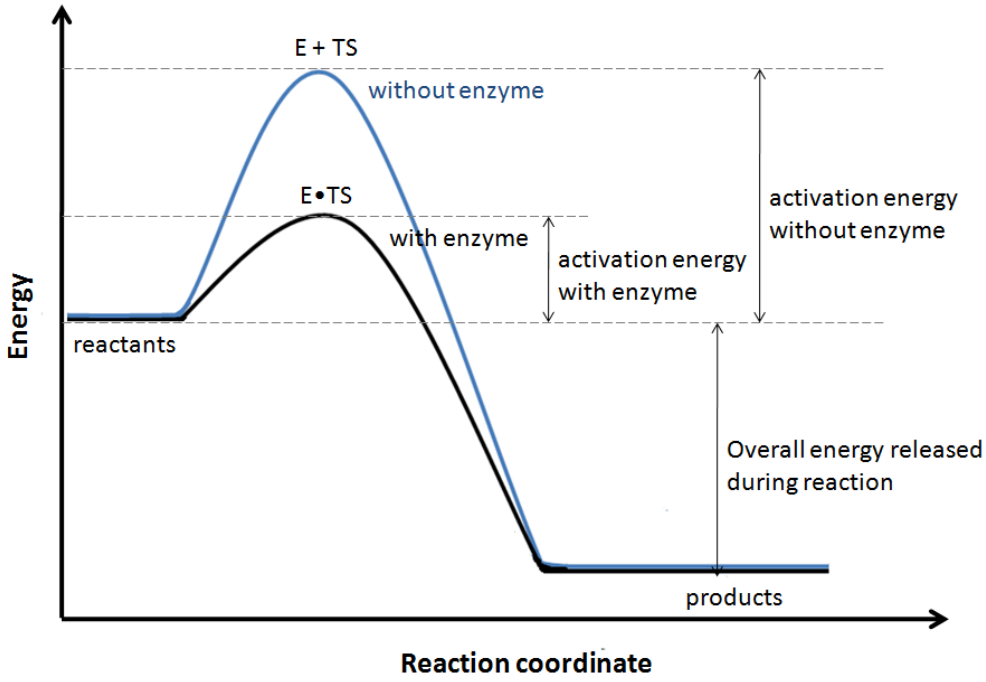

Figure 9. Enzymatic transition state stabilization[40].

Generally, enzymes bind to their substrates quickly; however, transition state inhibitors commonly exhibit a rapid weak binding first, followed by a subsequent slow tight-binding. Even though some tightly bound inhibitors have been explored with rapid onset, slow binding is still a common feature of the transition state inhibitors[40]. This phenomenon could be explained by the fact that the mimics are not as efficient activators as the substrates in inducing the transition state conformations of the enzyme. Besides the necessary conformational change, the enzymes also provide crucial electrostatic stabilization for the transition states in their solvent-restricted active site. As a result, the electrostatic features are also key criteria in the design of transition state mimics.

AroA's transition state structures

AroA's catalytic mechanism has been extensively studied for decades, but the transition state structures have not been elucidated yet. In the presence of 3, 4-dideoxy shikimate 3-phosphate (ddS3P), AroA is shown to be capable of catalyzing solvent tritium exchange into the methylene group of PEP[26]. Since ddS3P lacks the 5' hydroxyl group comparing to the enzyme's substrate S3P, the result indicates that protonation of the double bound in PEP does not require the nucleophilic addition by the 5' hydroxyl group of S3P, and also a cationic intermediate of PEP should be involved in a complete AroA catalysis.

Recent studies on enolpyruvyl reactivity from Berti group revealed that the catalytic imperative for AroA's reaction is to protonate C3 of PEP or EP-OR[41]. The catalytic imperative is the step in the reaction mechanism with the highest activation energy, and therefore requires the greatest catalytic power. The unactivated enolpyruvyl group of EPSP is not susceptible to nucleophilic attack even under extreme conditions, in 1 M KOH (pH 14) at 90 °C[41]. On the other hand, the nonenzymatic EPSP hydrolysis is significantly accelerated by acid catalysis, by $> 5 \times 10^8$ fold, implying that prior C3' protonation of enolpyruvyl group proceeds the nucleophilic attack at C2'[41]. Once the EPSP cation is formed, the subsequent nucleophilic attack has almost no energetic barrier. In TS analysis, previous students in Berti lab have demonstrated that AroA is capable of protonating C3 of EPSP and stabilizing the positive charge on the oxacarbenium ion intermediate during enzyme-catalyzed EPSP hydrolysis. In trapping

experiments, AroA is also shown to be capable of forming a discrete EPSP cation in its normal reaction pathway. Stabilizing such positively charged intermediates requires significant reaction energy, for > 15 kcal/mol[41], so it should be a reflection of the enzyme's intrinsic catalytic pathway. Thus we postulate that the enolpyruvyl group would carry a full positive charge at the transition state, and the TS structures in AroA catalysis should be oxacarbenium ion-like species (Figure 10).

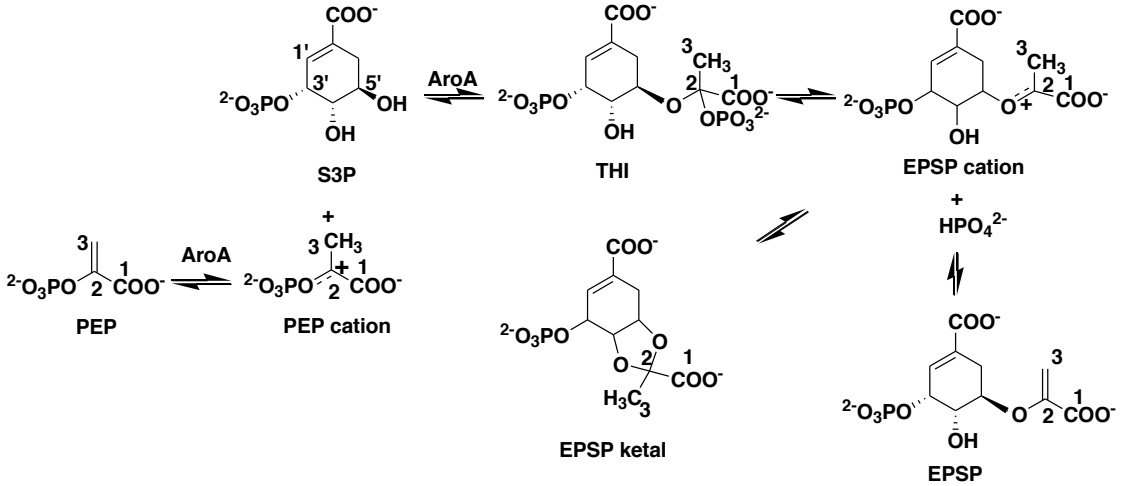

(A)

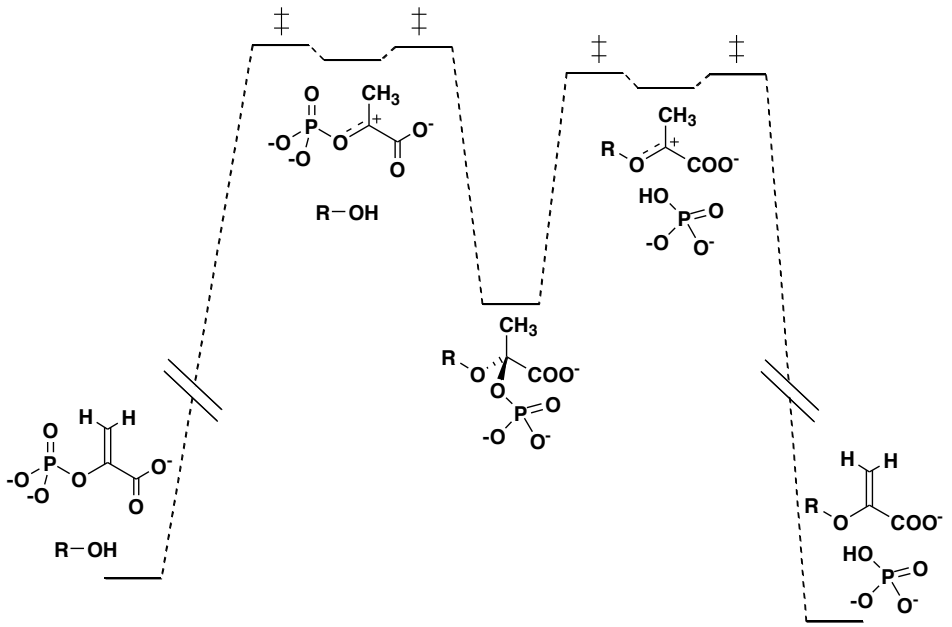

Figure 10. (A) AroA's catalysis, showing the putative oxacarbenium ion intermediates. (B) Energy diagram of AroA's catalysis. (Figure courtesy of Dr. Paul Berti)

DAHP synthase's transition state structures

DAHP synthase catalyzes the first committed step in the shikimate pathway, where the aldol condensation between PEP and erythrose 4-phosphate (E4P) leads to the formation of DAHP and inorganic phosphate (Figure 11)[42]. PEP binds to DAHP synthase first, followed by E4P. The *si* face of PEP C3 then stereospecifically attacks the *re* face of the C1 of E4P, forming a tetrahedral intermediate (THI)[43]. The elimination of phosphate proceeds through the unusual C-O bond cleavage[44], and DAHP is produced. DAHP synthase is active as a homotetramer[45], and its catalysis requires a divalent metal cofactor[46]. DAHP synthase is subject to feedback inhibition by its amino acid products[45].

DAHP synthase's catalytic mechanism has been proposed to start with PEP's methylene moiety nucleophilic attacking the aldehyde group of E4P, forming an oxacarbenium ion intermediate. This reaction results in a change of geometry around C2 of PEP, where the trigonal planar geometry in PEP is transformed into the tetrahedral geometry in the phosphohemiketal intermediate. The breakdown of THI is accomplished through C-O bond cleavage, with a second oxacarbenium ion species formed. 3-deoxy-*D*-manno-2-octulosonate-8-phosphate synthase (KDO8P synthase), the enzyme that catalyzes the condensation between PEP and *D*-arabinose-5-phosphate (A5P), shares several structural and mechanistic similarities with DAHP synthase[44]. The formation of the hemiketal biphosphate intermediate in KDO8P synthase's catalysis has been detected using mass spectrometry (ESI-MS)[47], which lends further credence to the formation of putative oxacarbenium ion intermediates. As a result, we postulate that the TS structures in DAHP synthase's catalysis should be oxacarbenium ion-like species. DAHP•oxime has been designed to mimic the structural and electrostatic features of the oxacarbenium ion intermediate (Figure 12). It has been determined to be a slow, tight-binding inhibitor with an ultimate K_i of 9×10^{-11} M^{2} [55].

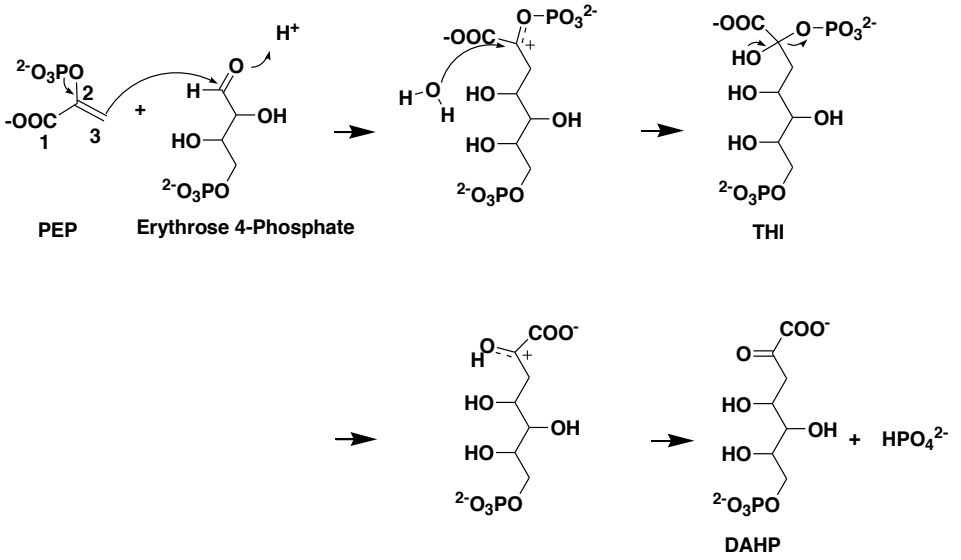

Figure 11. DAHP synthase's catalysis, showing putative oxacarbenium ion intermediates.

Fragment-based inhibitor design for AroA and DAHP synthase

Figure 12 demonstrates the library of oxacarbenium ion-like mimics we have proposed. The molecules will be utilized as inhibitors, and most importantly as mechanistic probes to investigate the catalytic functionalities of the enzymes. The putative oxacarbenium ion intermediate possesses a partial double bond between C2 of PEP and the bridging oxygen of phosphate. Using fragment-based approach, we modified the oxacarbenium ion scaffold with a variety of substituents. We introduced the ring moiety and various positively charged analogs into the library. Ideally, ddS3P will be used as a critical component in the combinatorial inhibitor, since it is capable of activating the enzyme for C3 protonation through the binding of the carboxylate and phosphate moieties, while simultaneously providing more physical space at the C5' position of ddS3P for optimum interaction between the oxacarbenium ion mimics and

enzyme. Repeated attempts to synthesis ddS3P have failed, but we will still be able to observe the interaction between the TS mimics and the enzyme, since PEP cation is formed in presence of S3P's 5' hydroxyl group in the normal catalytic cycle. For DAHP synthase, glycerol 3-phosphate and the oxacarbenium ion mimics will be used as combined inhibitors for the enzyme.

(A)

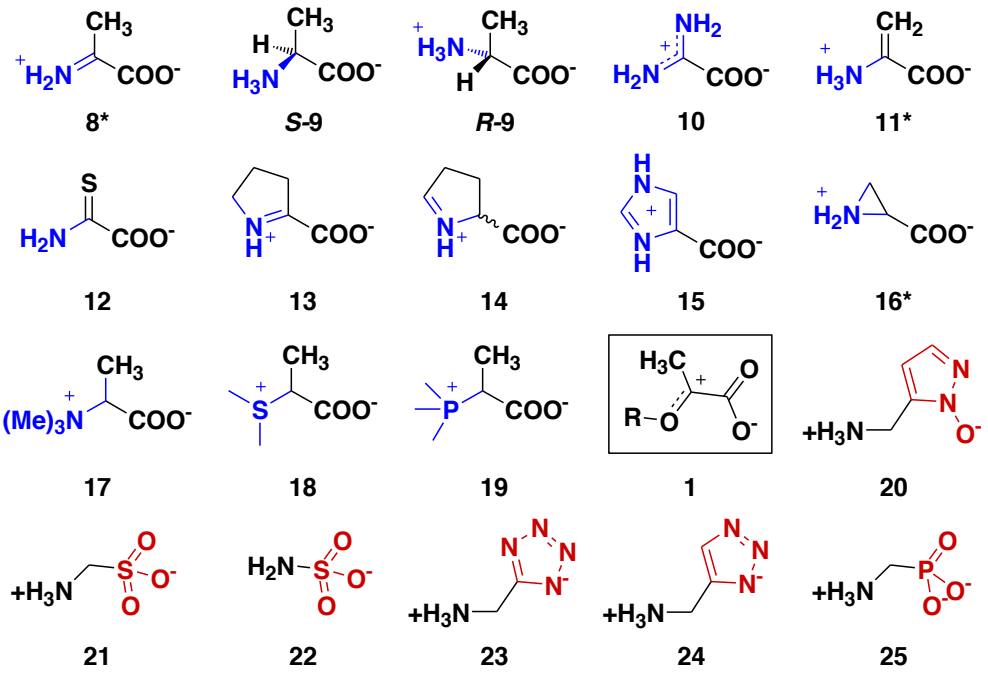

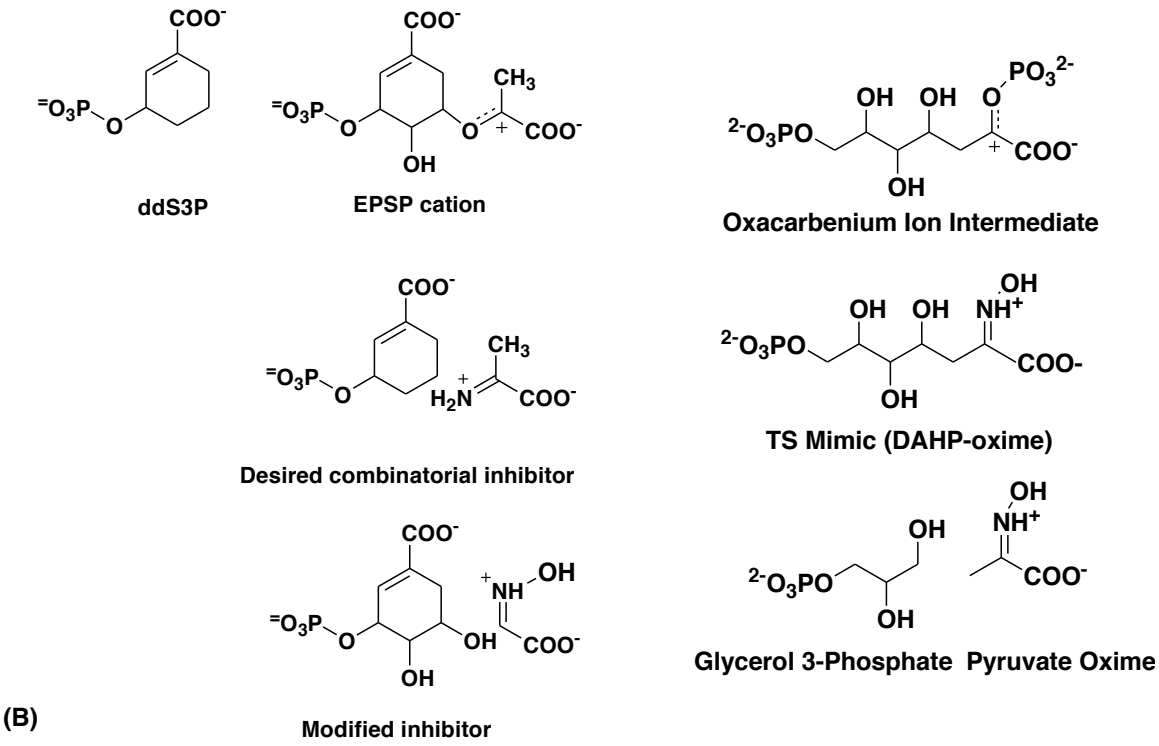

Figure 12. The library of oxacarbenium ion-like mimics, designed with fragment-based approach. (Figure courtesy of Dr. Paul Berti)

Objective of this project

This project is essentially composed by the characterization of *Borrelia burgdorferi* MurA, and the transition-state inhibitor design for AroA and DAHP synthase. The expression vector of Bb_MurA were created first, and then the expression condition of the enzyme was modified in order to obtain optimum purification yield and enzyme activity. Fosfomycin inhibition tests on the Bb_MurA D116C mutant were performed, since this can lend credence on the catalytic role Aps/Cys plays in the reaction. The molecules in the oxacarbenium ion library were synthesized, and then tested on the target enzymes. The comparison of different inhibition effect derived from each individual molecule elucidated effective binding moieties in the enzyme's active site, and provide invaluable evidence for discovering optimal TS inhibitors as novel antimicrobial agents.

Material and methods

General

Reagents were purchased from Sigma/Aldrich or Bioshop Canada, unless otherwise noted. Mono QTM 5/50 GL and chelating Sepharose columns were from GE Healthcare. HPLC chromatography was performed on a Waters system equipped with a dual UV wavelength detector.

Creation of purification vector with Bb_MurA gene

The *B. burgdorferi* MurA (Bb_MurA) gene was cloned from *B. burgdorferi* strain B31 genomic DNA (American Type Culture Collection). Several versions of this gene exist in Berti lab, including versions with alternate start codons (see Figure 4 and results), and *N*- and *C*-terminal His-tags. Another plasmid containing the "short form" with a TEV-cleavable *N*-terminal His-tag was created using Gateway™ technology (Invitrogen). All constructs were sequenced before expression.

Purification of Bb_MurAH6 and its mutant

The Bb_MurA plasmid was transformed by the heat shock method into *Escherichia coli* BL21*(DE3) cell containing Rosetta plasmid, plated on LB/agar plates (50 mg/L ampicillin, 17 mg/L chloramphenicol) plates. One overnight colony was transferred into 50 mL of selective LB media and incubated overnight with shaking at 37°C. The overnight culture was then added to two 1 L portions of selective LB media and incubated at 30 °C for 24 h without induction. The cells were harvested by

centrifugation at 5000 × *g* for 20 min, and all further steps were carried out at 4 °C. The cell pellet was resuspended in 30 mL wash buffer (50 mM Na-HEPES, pH 7, 150 mM NaCl), plus 20 mM imidazole, and by three passages through an EmulsifFlex-C5 high pressure homogenizer (Avestin) at 10,000 psi at 4°C. Lysed culture was centrifuged at 16,000 × *g* for 10 min. The supernatant was filtered at 0.2 µm and applied to a freshly charged Sepharose Fast Flow Ni^{2+} affinity column (GE Healthcare) at a rate of 1 mL/min. The loaded column was first washed with wash buffer containing 20 mM imidazole at the rate of 0.1 ml/min for 18 h, then with wash buffer plus 100 mM imidazole, and plus 200 mM imidazole. Bb_MurA was finally eluted in wash buffer plus 500 mM imidazole. The buffer was exchanged into storage buffer (50 mM Na-HEPES, pH 7, 650 mM NaCl, 1 mM DTT). Protein purity was checked by SDS-PAGE and protein concentration was from A_{280} or by Bradford assay (BioRad). The molar absorptivity, ε, of Bb_MurA was determined using the Edelhoch method[48].

Kinetic assay of Bb_MurA and its mutant

Reaction rates were measured in a 96-well plate format by detecting phosphate product formation with the Malachite Green/ammonium molybdate assay. Assays were conducted at 37 °C in 50 mM Na•HEPES, pH 7.0, 150 mM NaCl and 1 mM DTT. Substrate and enzyme solutions were incubated separately for 20 min, and then the reaction was started by adding enzyme to the substrate solutions. Aliquots of reaction mixture (50 µL) were added to 50 µL of MG/AM, followed by 10 µL 34% citrate solution 70 s later. A_{660}

was measured after 20 min. Under these conditions, catalytic activity of the enzyme was stable for up to 3 h.

Initial velocities were measured at high, fixed [UDP-GlcNAc] and varying [PEP], then with high, fixed [PEP] and varying [UDP-GlcNAc]. The fixed concentrations were 1.6 mM for Bb_MurA$_{H6}$, and 0.8 mM for Bb_MurA$_{H6}$(D116C). Rates were fitted to equation **1**:

$$\frac{v_0}{[\mathrm{E}]_0} = \frac{\dfrac{k_{\mathrm{cat}}[\mathrm{UDP\text{-}GlcNAc}][\mathrm{PEP}]}{K_{\mathrm{M,UDP\text{-}GlcNAc}}K_{\mathrm{M,PEP}}}}{1 + \dfrac{[\mathrm{UDP\text{-}GlcNAc}]}{K_{\mathrm{M,UDP\text{-}GlcNAc}}} + \dfrac{[\mathrm{PEP}]}{K_{\mathrm{M,PEP}}} + \dfrac{[\mathrm{UDP\text{-}GlcNAc}][\mathrm{PEP}]}{K_{\mathrm{M,UDP\text{-}GlcNAc}}K_{\mathrm{M,PEP}}}} \quad \textbf{(1)}.$$

Equation 1 assumes a random sequential mechanism for two substrates, as used for the homologous enzyme AroA[7].

($k_{cat}/K_M)_{UDP\text{-}GlcNAc}$ was determined by direct fitting to equation 2:

$$\frac{v_0}{[\mathrm{E}]_0} = \frac{\left(\dfrac{k_{cat}}{K_M}\right)_{\mathrm{UDP\text{-}GlcNAc}} \dfrac{[\mathrm{UDP\text{-}GlcNAc}][\mathrm{PEP}]}{K_{\mathrm{M,PEP}}}}{1 + \dfrac{[\mathrm{UDP\text{-}GlcNAc}]}{K_{\mathrm{M,UDP\text{-}GlcNAc}}} + \dfrac{[\mathrm{PEP}]}{K_{\mathrm{M,PEP}}} + \dfrac{[\mathrm{UDP\text{-}GlcNAc}][\mathrm{PEP}]}{K_{\mathrm{M,UDP\text{-}GlcNAc}}K_{\mathrm{M,PEP}}}} \quad \textbf{(2)},$$

and ($k_{cat}/K_M)_{PEP}$ by suitable modification of equation 2.

Fosfomycin titration on Bb_MurA D116C

For the time-dependent titration, 2 µM Bb_MurA was pre-incubated with 0.2 mM fosfomycin and 2 mM UDP-GlcNAc for defined time periods, then equal volume of 2 mM PEP was added to start the reaction. Residual activity was measured at as short time as possible to minimize the increase in covalent inhibition during the course of the assay.

Under these pre-incubation conditions, the enzyme was saturated with both UDP-GlcNAc and fosfomycin, so k_{inact} could be calculated from the first order decrease in residual activity as a function of pre-incubation time, equation **3**:

$$v_{0,\text{residual}} = V_{\max} \times \mathrm{e}^{-k\text{inact}\times\text{t}} + c \qquad (\mathbf{3}).$$

The constant term, *c*, accounted for the residual activity, ~9%, present after extended pre-incubation with fosfomycin.

In order to determine the dissociation constant, K_i, of fosfomycin binding, fosfomycin was pre-incubated with UDP-GlcNAc for 10 min, then added to a mixture of Bb_MurA D116C and PEP to give final concentrations of up to 10 mM fosfomycin, 1 mM UDP-GlcNAc, 1 µM Bb_MurA D116C, and 1 mM PEP.

Fosfomycin binding is uncompetitive with respect to UDP-GlcNAc and competitive with respect to PEP (Scheme 1). For uncompetitive inhibition, $K_{i,apparent} = K_{i,true}$ when [substrate] >> K_M. As [UDP-GlcNAc] was 1 mM (48 × $K_{M,UDP\text{-}GlcNAc}$), it could be neglected, and only PEP was included in fitting to the competitive inhibition equation **4** to K_i:

$$v_0 = \frac{V_{max}[\mathrm{PEP}]}{K_{\mathrm{M,PEP}}\left(1+\frac{[\text{fosfomycin}]}{K_i}\right)+[\mathrm{PEP}]} \quad \textbf{(4).}$$

pH profile of Bb_MurA

The pH profile was generated using the enzyme purified with extended washing. The k_{cat} at each pH condition was determined by running reactions at 37 °C with saturating substrate concentrations, 1.6 mM, in 150 mM NaCl, 1 mM DTT and 50 mM buffer component: potassium acetate (pH 4.5, 5), K·MES (pH 5.5, 6), Na·HEPES (pH 7, 7.5), and Tris·HCl (pH 8 and 9). Rates were fitted to equation **5**:

$$\frac{v_0}{[\mathrm{E}]_0} = \frac{k_{\mathrm{cat,max}} \times 10^{\mathrm{pH}-\mathrm{p}K_{\mathrm{a}1}} \times 10^{\mathrm{p}K_{\mathrm{a}2}-\mathrm{pH}}}{(10^{\mathrm{pH}-\mathrm{p}K_{\mathrm{a}1}}+1)\times(10^{\mathrm{p}K_{\mathrm{a}2}-\mathrm{pH}}+1)} \quad (\textbf{5}).$$

Pyruvate oxime and glyoxylate oxime synthesis

In order to synthesis pyruvate oxime, equal amounts of pyruvate and $NH_2OH{\cdot}HCl$ were combined, and one equivalent of NaOH was added to neutralize the acid. The formation of pyruvate oxime was detected by anion exchange chromatography using a MonoQ column (Amersham, 5 × 50 mm) with UV absorbance detection at 205 nm and 230 nm, and solvent program in Table 1. HPLC results showed that the reagents had been consumed completely, and the purity of pyruvate oxime is confirmed by NMR.

Glyoxylic oxime is synthesized using the same procedure, by mixing glyoxylic acid, $NH_2OH{\cdot}HCl$ and NaOH with the ratio of 1:1:1 in ddH_2O. The purity of the product was confirmed by NMR.

Table 1. Solvent program for analytical HPLC of pyruvate oxime formation; A = 10 mM ammonium acetate; B= 200 mM ammonium acetate.

Time (min.)	Flow rate (ml/min)	%A	%B
0	0.5	100	0
4	0.5	100	0
44	0.5	0	100
50	0.5	0	100

Inhibition test on Bb_MurA and Ec_AroA

E. coli AroA and its substrate S3P were synthesized according to reference [7]. The inhibition assays for Bb_MurA and Ec_AroA were conducted by adding the mixture of substrates and designated amounts of inhibitor into the pre-incubated enzyme solution. The reaction conditions for Bb_MurA are the same as described earlier. The reactions conditions for Ec_AroA are from reference [7]. Residual rate is determined by detecting phosphate formation in MG/AM assay.

Inhibition test on DAHP synthase

E4P and DAHP synthase were obtained from Naresh Balachandran in the Berti Lab. All small molecules and glycerol 3-Pi were tested individually on DAHP synthase first. Then the enzyme was tested with the combined inhibitors of glycerol 3-phosphate and

oxacarbenium ion mimics. In order to determine the dissociation constant, K_i, of the inhibitor's binding, the residual rate of DAHP synthase was detected when the concentration of oxacarbenium ion molecules varied from 0 mM to 150 mM. The reaction was conducted at 25 °C and the mixture contained 20 nM DAHP synthase, 100 or 300 µM PEP, 100 or 300 µM E4P and 4 µM Mn^{2+}, 200 µM TCEP and 0.25 mg/ml BSA. The reaction buffer is composed by 50 mM Na·HEPES, 100 mM NaCl, pH 7.0.

DAHP synthase's catalysis follows an ordered mechanism, with E4P binding first and followed by PEP[49]. The data derived with glycerol 3-phosphate & pyruvate oxime/glyoxylate oxime was fitted into equation **6**:

$$\frac{v_0}{[\mathrm{E}]_0} = \frac{k_{\mathrm{cat}}[\mathrm{A}][\mathrm{B}]}{K_{\mathrm{MA}}K_{\mathrm{MB}}\left(1+{}^{[\mathrm{I}]}/_{K_{\mathrm{i}}}\right)+[\mathrm{A}]K_{\mathrm{MB}}+[\mathrm{A}][\mathrm{B}]} + \mathrm{offset} \qquad \textbf{(6)},$$

where the offset represents the residual rate observed with excessive inhibitor.

4-Imidazolecarboxylic acid was expected to bind to the DAHPS•Mn^{2+}•E4P complex, thus we suspect its binding is competitive with respect to PEP, and uncompetitive with respect to E4P and Mn^{2+}. The kinetic data derived with 4-imidazolecarboxylic acid was fitted into both equation **7**:

$$\frac{\mathrm{v}_0}{[\mathrm{E}]_0} = \frac{k_{\mathrm{cat}}[\mathrm{A}][\mathrm{B}][\mathrm{C}]}{K_{\mathrm{A}}K_{\mathrm{B}}K_{\mathrm{C}}+[\mathrm{A}]K_{\mathrm{B}}K_{\mathrm{C}}+[\mathrm{A}][\mathrm{B}]K_{\mathrm{C}}\left(1+{}^{[\mathrm{I}]}/_{K_{\mathrm{i}}}\right)+[\mathrm{A}][\mathrm{B}][\mathrm{C}]} \qquad \textbf{(7)},$$

where complete inhibition is eventually achieved; and equation 8:

$$\frac{\mathrm{v_0}}{[\mathrm{E}]_0} = \frac{k_{\mathrm{cat}}[\mathrm{A}][\mathrm{B}][\mathrm{C}]}{K_{\mathrm{A}}K_{\mathrm{B}}K_{\mathrm{C}}+[\mathrm{A}]K_{\mathrm{B}}K_{\mathrm{C}}+[\mathrm{A}][\mathrm{B}]K_{\mathrm{C}}\left(1+{}^{[\mathrm{I}]^2}\!/_{K_{\mathrm{i}}{}^2}\right)+[\mathrm{A}][\mathrm{B}][\mathrm{C}]} \quad \textbf{(8)},$$

where the binding of inhibitor is cooperative.

Inhibition type determination of 4-imidazolecarboxylic acid against PEP, E4P and Mn^{2+}

In order to determine the inhibition type of 4-imidazolecarboxylic acid against PEP, the concentration of E4P and Mn^{2+} were kept constant, at 100 µM and 4 µM respectively, while the concentration of PEP varied from 0-10 mM. The residual rates of 20 nM DAHP synthase were determined using MG/AM assay, when various concentrations of inhibitor were present. The data was plotted into Lineweaver-Burke plot.

E4P causes significant substrate inhibition towards DAHP synthase, which could be reflected by the decreased enzymatic rate when more than 100 µM E4P was present. When determining 4-imidazolecarboxylic acid's inhibition type against E4P, the concentrations of PEP and Mn2+ were kept constant, at 100 µM and 4 µM, while the concentration of E4P was varied from 0 to 90 µM.

For the determination with respect to Mn^{2+}, the concentrations of PEP and E4P were kept both at 100 µM, and the concentration of Mn^{2+} was varied from 0 to 40 µM.

Bb_MurA start codon determination

Wild-type long-form and short-form Bb_MurA genes were incorporated into *Escherichia coli* BL21*(DE3) cell respectively, and the proteins were expressed following the non-inducing routine. The obtained pellets were resuspended in buffer containing 50 mM Na·HEPES, 150 mM NaCl, pH 7.0 and stored at -20 °C. The cells were chemically lysed with CelLytic, the pellets removed by centrifugation, and the supernatant added to SDS loading-dye.

In order to obtain the native MurA, *Borrelia burgdorferi* was cultured in the Biosafty Level 2 lab at 30 °C based on cultures from Dr. George Chaconas (University of Calgary). *B.burgdorferi* cultures were harvested by centrifugation at 3 700 g for 15 minutes and the cell pellet was stored at -20°C.

A 16.5 × 22 cm 5% to 15% gradient SDS-gel was casted. Both versions of Bb_MurA standard were loaded onto the gel, as well as the resuspension of *B.burgdorferi* cell pellet. The electrophoresis was performed, followed by Western blotting.

Results

Start codon

The MurA gene in *B. burgdorferi* has two potential start codons: a GTG codon, followed by an ATG 15 codons downstream (Figure 4). GTG normally codes for Val, but is used by some bacteria as a start codon. We will refer to the gene starting from Val as "long-form" Bb_MurA, and the gene starting from Met as "short-form" Bb_MurA. The true start codon is not yet known.

Purification of Bb_MurA

Due to the poor stability of the wild type enzyme, both *N*- and *C*-terminal His-tags have been used. Protein expression levels with IPTG induction were typically 0.3 mg/L, with large amounts of insoluble Bb_MurA remaining in the cell pellet after lysis. Leaky expression was then attempted to solve this issue. By culturing cells at 30 °C for 24 h without adding IPTG, the yield was increased to ~10 mg/1 L of cell culture. Eluted fractions were monitored on SDS-PAGE to confirm purity (Figure 13).

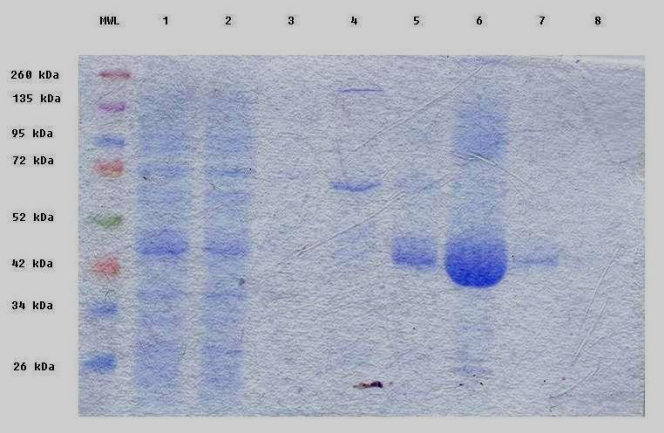

Figure 13. Bb_MurA$_{H6}$ purification, followed by 13% SDS-PAGE. MWL=molecular weight ladder; (1) cell lysate; (2) column flow through; (3) overnight 0mM imidazole wash; (4) 100mM imidazole wash; (5) 200mM imidazole wash; 500 mM imidazole elution: (6) fraction #1 (7) fraction #4; (8) fraction #7.

Steady-state kinetic parameters

Initial kinetic assays with Bb_MurA$_{H6}$ yielded an extremely low k_{cat} value of 0.041 ± 0.002 s^{-1}. This was consistent with k_{cat} values obtained by several students in the lab, but much lower than that obtained by Menat Attia in 2006. In an attempt to resolve this discrepancy, we then optimized the purification conditions by washing the protein-loaded Ni^{2+} column overnight at a low flow rate, in order to remove any non-covalently bound proteins or small molecules that could inhibit the protein. Bb_MurA purified in this way yielded a k_{cat} value up to 0.74 ± 0.01 s^{-1}, roughly 15-fold higher than the previous rate (Figure 14).

Table 2. Kinetic parameters of Bb_MurA$_{H6}$ and its D116C mutant.

pH=7.0	Bb_MurA$_{H6}$ (short-form)	Bb_MurA$_{H6}$(D116C) (short-form)	Bb_MurA$_{H6}$ (long-form)
k_{cat} (s^{-1})	0.57 ± 0.03	0.030 ± 0.003	0.74 ± 0.01
$(k_{cat}/K_M)_{PEP}$ ($M^{-1}\bullet s^{-1}$)	9.07(±0.05)×10^3	3.1(±0.8)×10^3	1.92 (± 0.03) ×10^4
$(k_{cat}/K_M)_{UDP\text{-}GlcNAc}$ ($M^{-1}\bullet s^{-1}$)	1.0 (±0.3)×10^4	1.7(±0.3)×10^3	3.09 (± 0.03) ×10^3
$K_{M,PEP}$ (μM)	66±9	11±2	39
$K_{M,UDP\text{-}GlcNAc}$(μM)	56±11	16±6	24

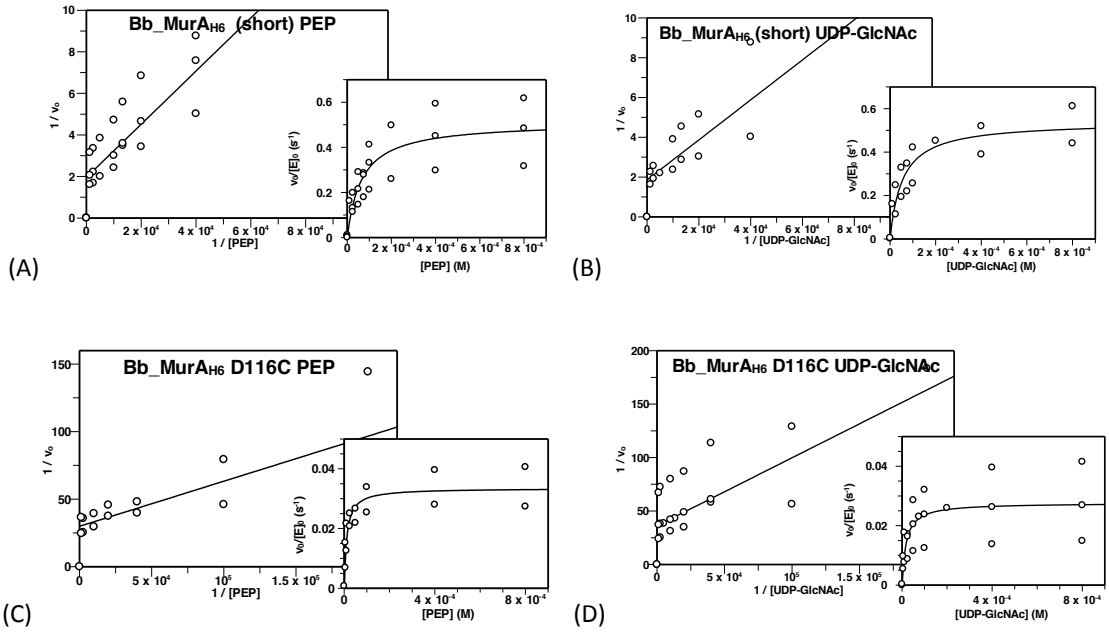

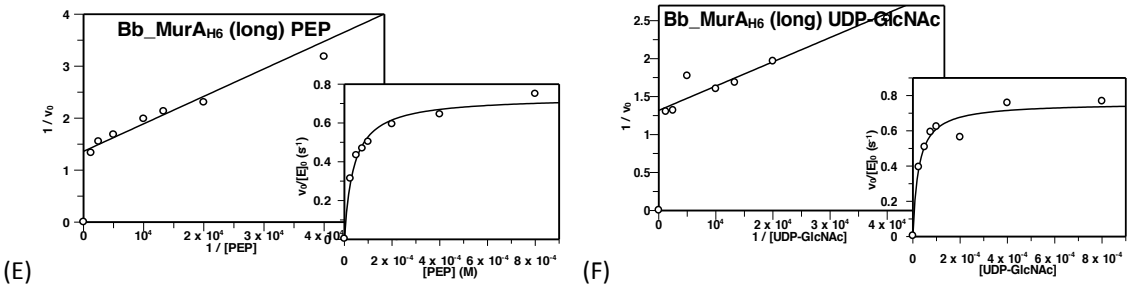

Figure 14. The steady-state kinetic parameters for Bb_MurA$_{H6}$ short-form with substrates (A) PEP and (B) UDP-GlcNAc, the D116C mutant with (C) PEP and (D) UDP-GlcNAc, and Bb_MurA$_{H6}$ long-form with (E) PEP and (F) UDP-GlcNAc.

Fosfomycin titration

Natively Asp-containing Bb_MurA is fosfomycin resistant, as expected, but in the presence of UDP-GlcNAc, Bb_MurA D116C exhibited time-dependent fosfomycin inactivation. After ~15 min incubation, inhibition is nearly complete, with < 10% residual activity. This residual activity, which is normally detected by phosphate formation in the MG/AM assay, was confirmed by following EP-UDP-GlcNAc formation using HPLC (data not shown). The rate of covalent modification, k_{inact}, was determined to be $0.021 \pm 0.003\ s^{-1}$ (Figure 15).

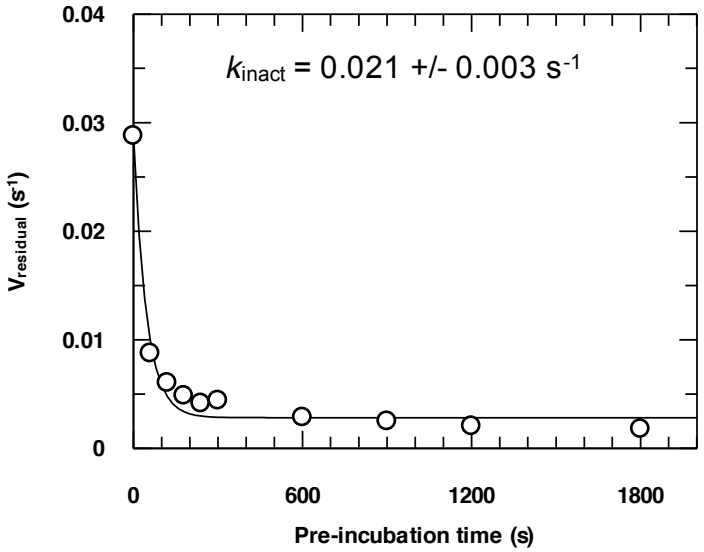

Figure 15. Time-dependent inactivation of fosfomycin to Bb_MurA D116C. The k_{inact} value was determined to be 0.021 ± 0.003 s^{-1}.

Without pre-incubation, the dissociation constant for fosfomycin's binding was 5.7 ± 0.4 μM (Figure 16). The fosfomycin concentration required for 50% inhibition was much greater than K_i, since the concentration of the competitive substrate, PEP, was much greater than its K_m.

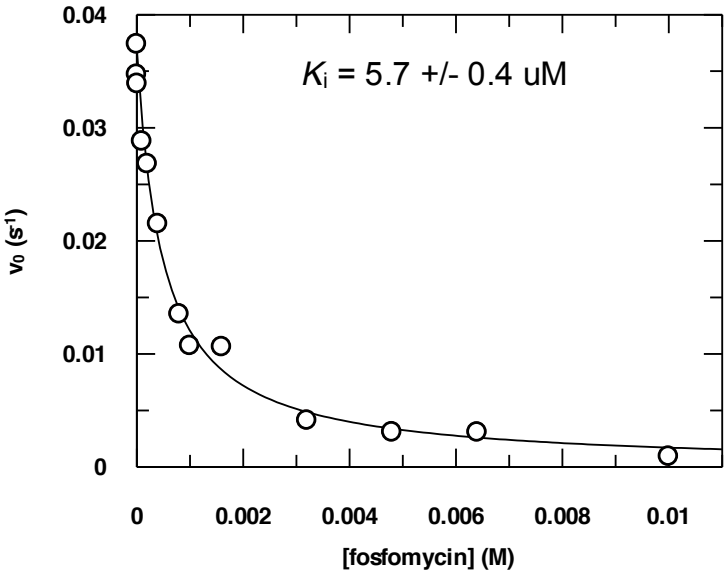

Figure 16. The K_i value of fosfomycin's alkylation towards Bb_MurA D116C was 5.7 ± 0.4 μM.

pH profile of short-form and long-form MurA

The pH versus k_{cat} profiles for three versions of Bb_MurA were determined. Substrate concentrations were saturating, so the rates reflected k_{cat}. The pH profile of the short-form enzyme had been determined previously with Bb_MurA that contained a non-covalently bound inhibitor (shown as the black dots with error bars in Figure 17A). By determining a partial pH-profile using fully active enzyme, it was possible to normalize the data in previously measured pH profile (shown as the maroon dots in Figure 17A). The pH profile for long-form Bb_MurA was also determined. Slight shifts are observed both in the acidic and basic limbs. The profile for short-form enzyme is slightly broader than the long-form enzyme. The pH profile for Bb_MurA D116C was previously determined by Meghann E. Gilpin in 2007. The pK_{a2} value shifted from around 7.0 in the wild-type enzyme to a value > 11 in the mutant.

Table 3. pK_a values determination for three versions of Bb_MurA.

	Bb_MurA (short-form)	Bb_MurA (long-form)	Bb_MurA D116C
pK_{a1}	3.8 ± 0.2	4.8 ± 0.1	3.5 ± 0.3
pK_{a2}	7.4 ± 0.2	7.1 ± 0.1	> 11

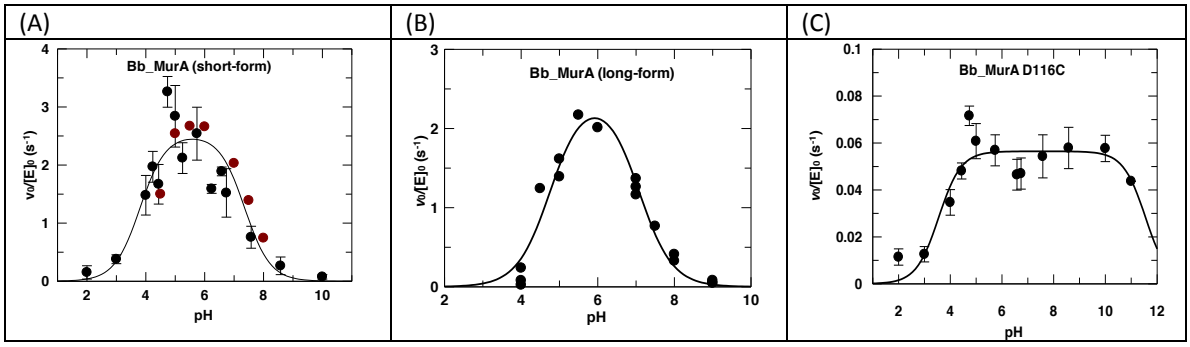

Figure 17. pH profiles for (A) Bb_MurA short-form, (B) Bb_MurA long-form and (C) Bb_MurA D116C.

Synthesis of pyruvate oxime and glyoxylate oxime

Pyruvate oxime synthesis was followed by ^{1}H-NMR, as the methyl group shifted upfield from δ=2.334 ppm in pyruvate to δ=1.959 ppm in pyruvate oxime. The reagents are consumed completely, as reflected in the NMR spectra and the HPLC chromatograms (Figure 18).

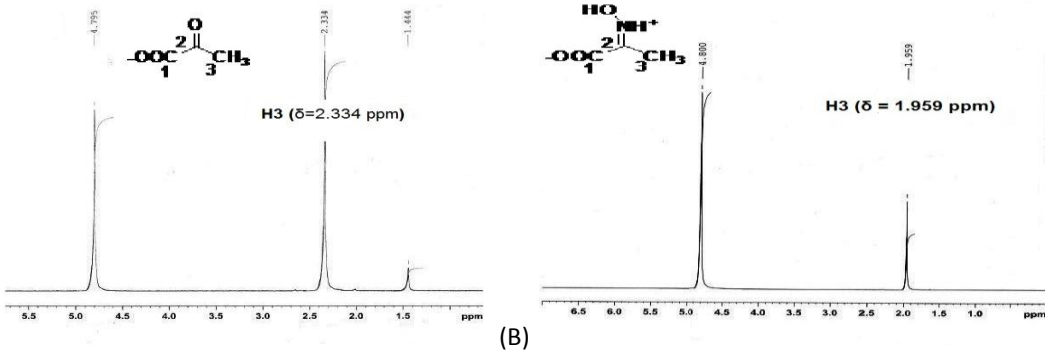

(A) (B)

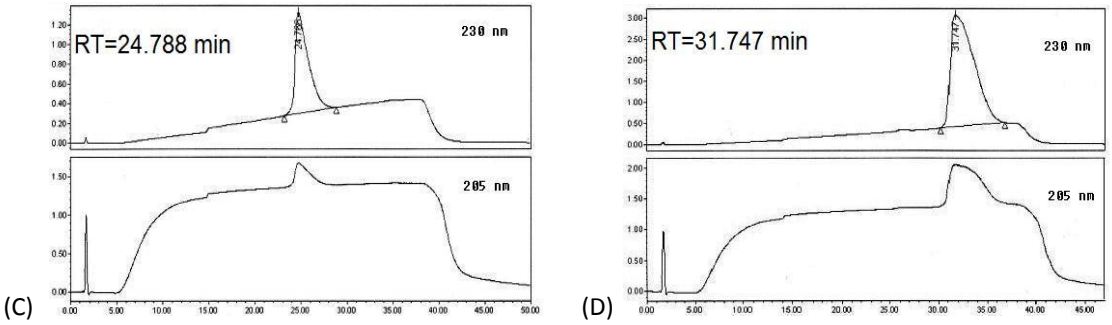

(C) (D)

Figure 18. NMR spectrums of (A) pyruvate and (B) pyruvate oxime; HPLC chromatograms of (C) pyruvate and (D) pyruvate oxime.

The formation of glyoxylate oxime was also confirmed by ^{1}H-NMR. The δ=5.281 ppm peak represents the proton on the hydrated aldehyde in glyoxylic acid, and the δ=7.512 ppm peak is the proton attached to the C=N bond in glyoxylate oxime.

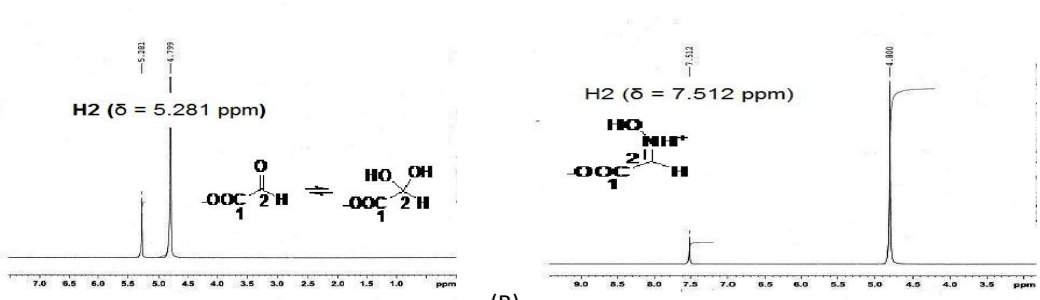

(A) (B)

Figure 19. NMR spectrums of (A) glyoxylic acid and (B) glyoxylate oxime.

Inhibition tests of pyruvate oxime and glyoxylate oxime on Bb_MurA and Ec_AroA

No apparent inhibition was observed on either enzyme with up to 5 mM inhibitors (Figure 20). Elongated incubation time does not promote better binding (Figure 21).

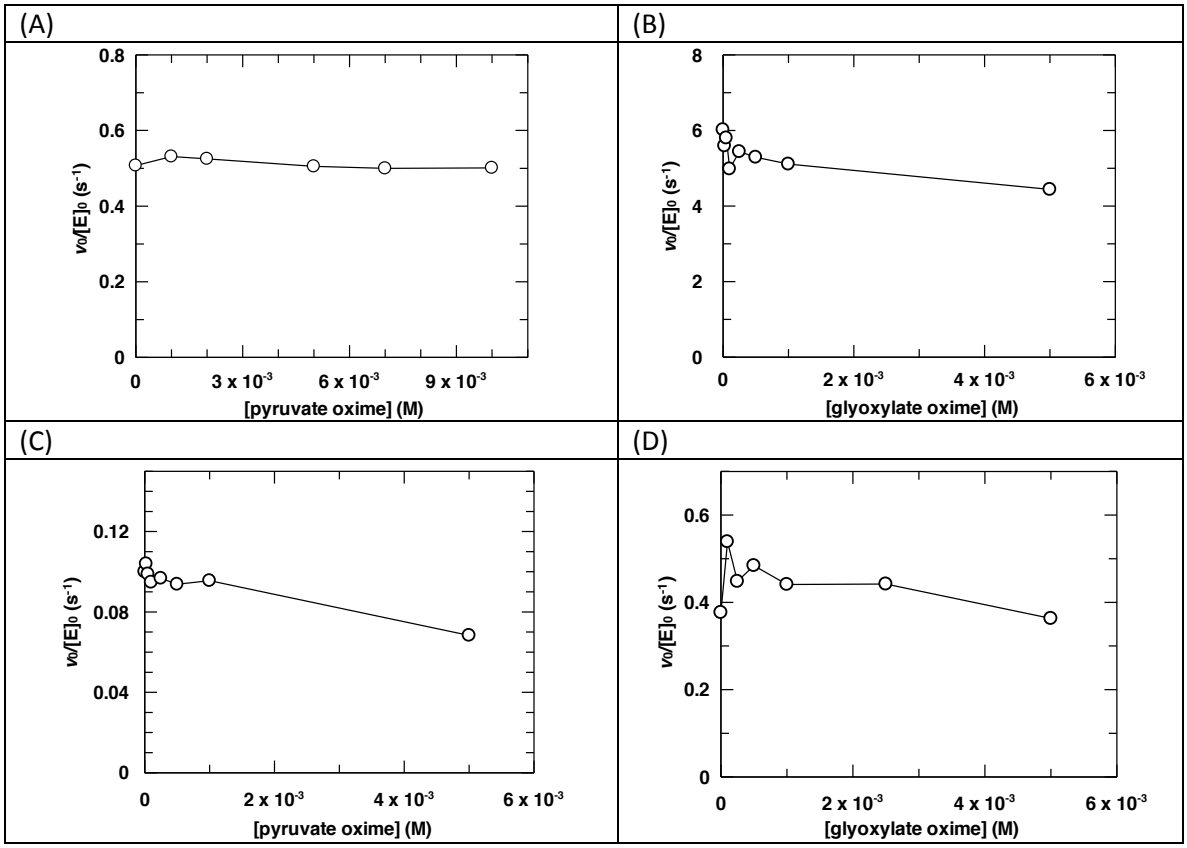

Figure 20. (A) Pyruvate oxime inhibition test on Ec_AroA; (B) Glyoxylate oxime inhibition test on Ec_AroA; (C) Pyruvate oxime inhibition test on Bb_MurA; (D) Glyoxylate oxime inhibition test on Bb_MurA.

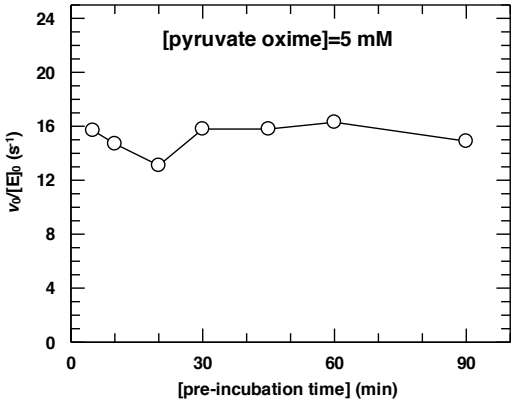

Figure 21. Time-dependent inactivation of pyruvate oxime towards Ec_AroA

Glycerol 3-phosphate & pyruvate oxime and glyoxylate oxime inhibition tests on DAHP synthase

Glycerol 3-phosphate exerts a modest inhibitory effect on DAHP synthase. Because the glycerol 3-phosphate sample brings along 3 mole % Pi absorbance in the background, we were unable to detect its effect on the enzyme at concentrations higher than 4 mM in MG/AM assay. Pyruvate oxime alone has no inhibitory effect on DAHP synthase, but the enzymatic rate decreased significantly when glycerol 3-phosphate is present. This is also observed for glyoxylate oxime, that the optimum inhibition is achieved only with the combination of glycerol 3-phosphate and the oxacarbenium ion mimics. Thus 4 mM glycerol 3-phosphate was utilized later to detect the binding affinity of the oxacarbenium ion molecules to DAHP synthase.

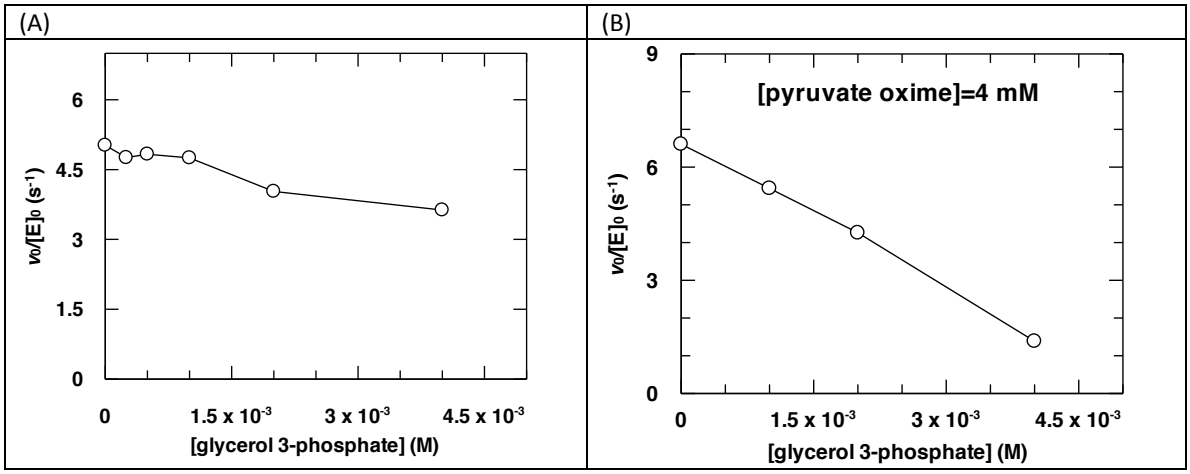

Figure 22. Glycerol 3-phosphate's effect on DAHP synthase, either (A) by itself, or (B) with the presence of 4mM pyruvate oxime.

In the presence of glycerol 3-phosphate, the enzymatic activity decreased as a function of the concentration of pyruvate oxime and glyoxylate oxime, with fitted K_i

values of 7.6 (± 0.9) × 10^{-5} M and 7.4 (± 1.7) × 10^{-5} M, respectively. The concentrations of both substrates utilized in the inhibition assay were more than 15-fold above their K_M values, so the inhibitor concentrations required for 50% inhibition were much greater than K_i values. Comparing to the significant background absorbance due to 4 mM glycerol 3-phosphate, the absorbance change reflecting the inhibited rate is relatively small, causing the rate data relatively noisy. Nevertheless, the overall trend is clear, so the K_i values obtained should be the true reflection of the inhibitors' affinity for the enzyme. The inhibition of glyoxylate oxime needs further characterization, where the residual rate of the enzyme is detected when 50 mM ~ 200 mM inhibitor is present.

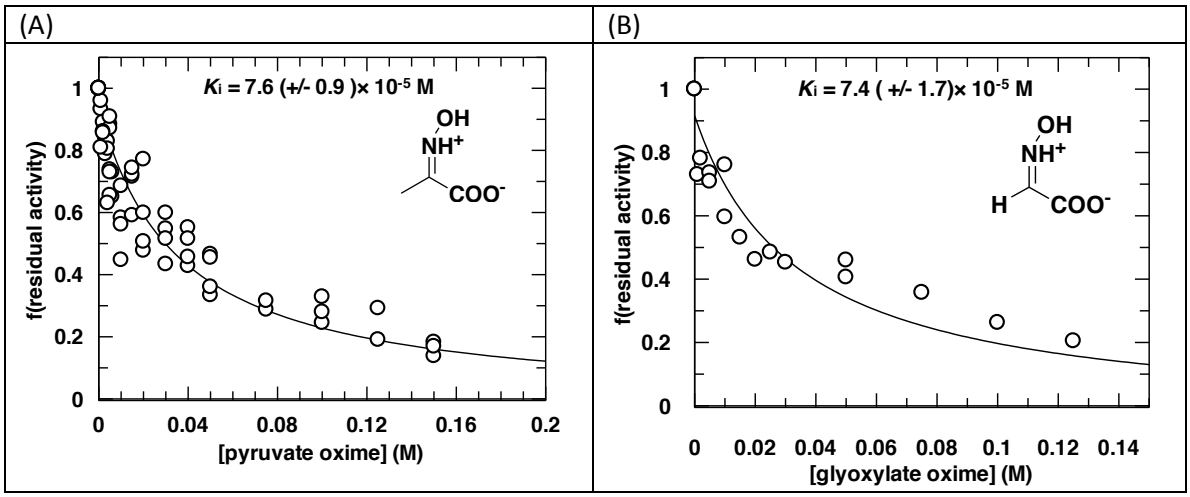

Figure 23. K_i determination of pyruvate oxime and glyoxlate oxime inhibition of DAHP synthase, in the presence of 4 mM glycerol 3-phosphate. (A) K_i of pyruvate oxime binding is 7.6 (± 0.9) × 10^{-5} M. (B) K_i of glyoxylate oxime binding is 7.4 (± 1.7) × 10^{-5} M.

R-alanine, *L*-alanine, sulfamic acid and aminomethanesulfonic acid inhibition test on DAHP synthase

No apparent inhibition was observed on DAHP synthase with any inhibitor above (Figure 24).

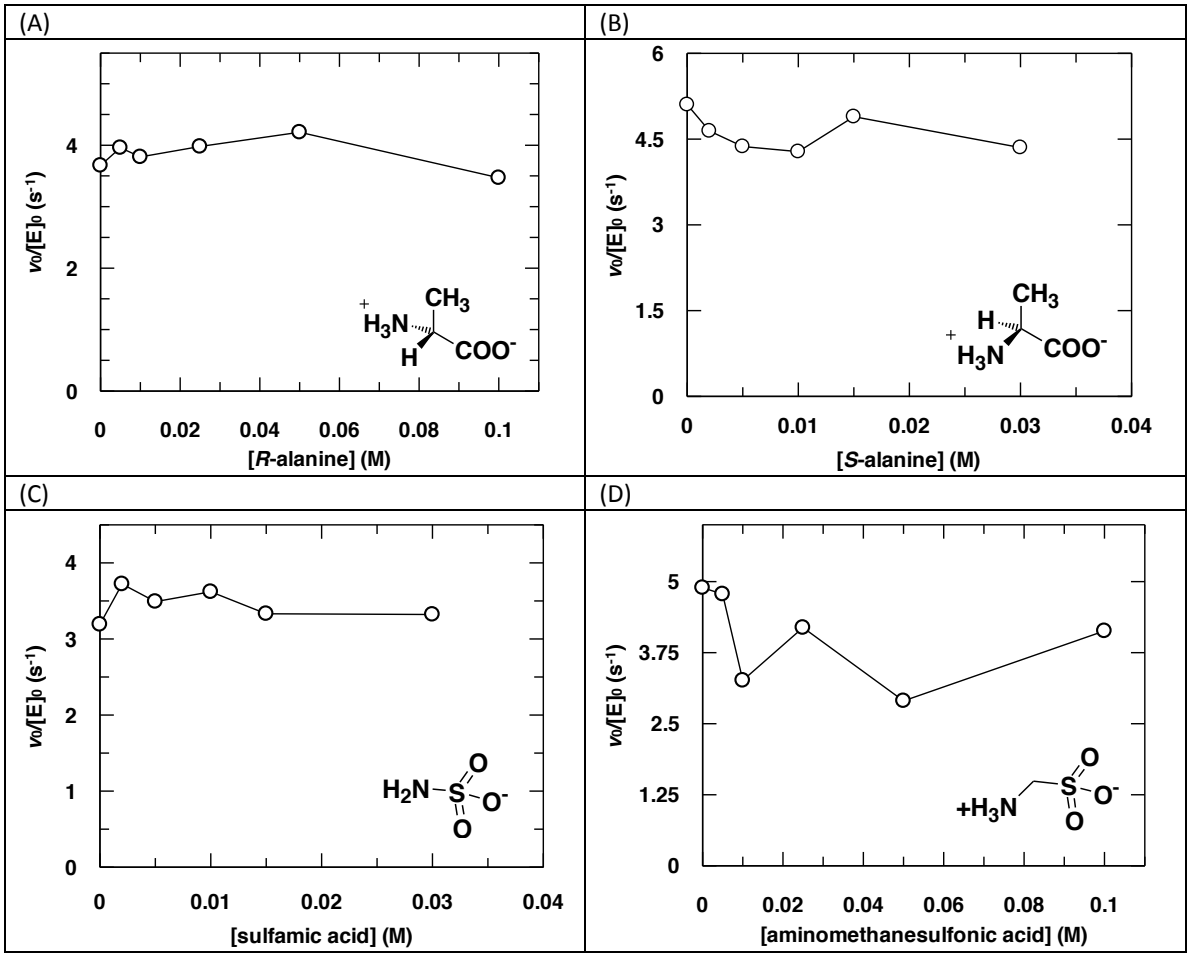

Figure 24. (A) *R*-alanine inhibition test on DAHP synthase; (B) *L*-alanine inhibition test on DAHP synthase; (C) sulfamic acid inhibition test on DAHP synthase; (D) aminomethanesulfonic acid inhibition test on DAHP synthase. All inhibition assays were performed in presence of 3 mM glycerol 3-phosphate.

4-Imidazolecarboxylic acid inhibition test on DAHP synthase

Imidazole carboxylic acid inhibition was better modeled by the equation that takes cooperativity into account (eq. **8**), both in the presence or absence of glycerol 3-phosphate (Figure 25). Thus we conclude that 4-imidazolecarboxylic acid's inhibition towards DAHP synthase should be cooperative, with fitted K_i values of 3.0(± 0.2) × 10^{-3} M by 4-imidazolecarboxylic acid alone, and 1.7(± 0.2) × 10^{-3} M by the combination of 4-imidazolecarboxylic acid and glycerol 3-phosphate. The inhibition occurs instantly, with

no pre-incubation time needed (Figure 27). The presence of glycerol 3-phosphate exerts a minor contribution to the inhibition, but not significant enough to effect the K_i value or the inhibition pattern (Figure 26). Imidazole alone causes no inhibition to the enzyme (data not shown).

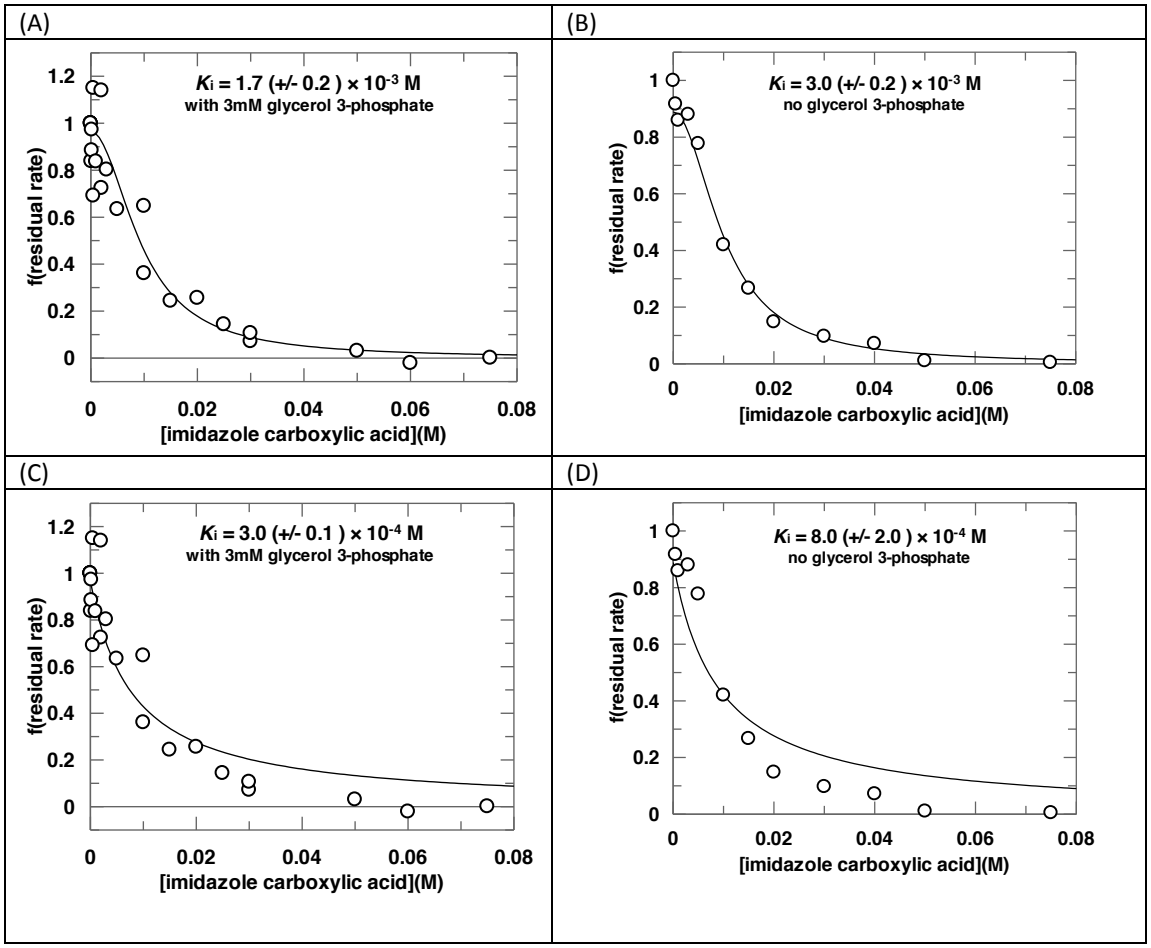

Figure 25. K_i determination of (A) 4-imidazolecarboxylic acid & glycerol 3-phosphate (Assuming the binding is cooperative, data was fitted into equation **8**. K_i was 1.7(± 0.2) × 10^{-3} M), and (B) 4-imidazolecarboxylic acid (Assuming the binding is cooperative, data was fitted into equation **8**. K_i was 3.0(± 0.2) × 10^{-3} M), towards DAHP synthase. K_i determination of (C) 4-imidazolecarboxylic acid & glycerol 3-phosphate (Assuming the binding is not cooperative, data was fitted into equation **7**. K_i was 3.0 (± 0.1) × 10^{-4} M), and (D) 4-imidazolecarboxylic acid (Assuming the binding is not cooperative, data was fitted into equation **7**. K_i was 8.0 (±2.0) × 10^{-4} M), towards DAHP synthase.

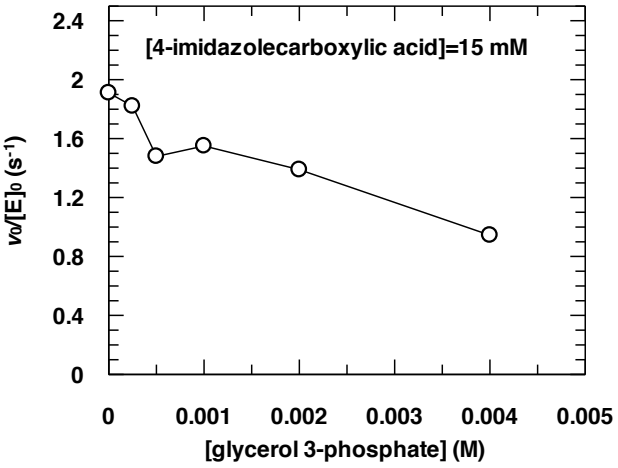

Figure 26. Glycerol 3-phosphate's effect on DAHP sythase when 4-imidazolecarboxylic acid is present.

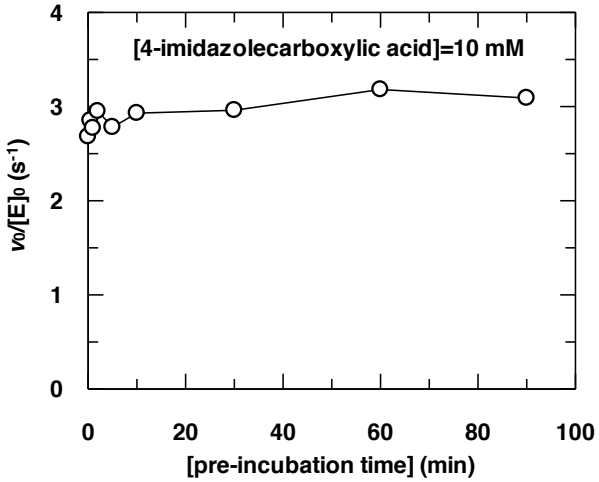

Figure 27. Time-depedent inactivation of 4-imidazolecarboxylic acid to DAHP synthase.

Inhibition type determination of 4-imidazolecarboxylic acid against PEP, E4P and Mn^{2+}

In order to determine the mode of inhibition (competitive, non- or uncompetitive) with respect to each substrate, initial velocities were measured while varying the

inhibitor concentration, [I], and one of the substrate concentrations, [PEP] (Figure 27), [E4P] (Figure 28) or [Mn^{2+}] (Figure 29).

With increased concentration of 4-imidazolecarboxylic acid, the K_M of PEP increased, from 26 μM to more than 200 μM, indicating decreased binding affinity (Table 4). The corresponding k_{cat} values gradually decreased, with vast lost of activity occurred when 25 mM inhibitor was utilized.

The fitted values of K_M values for E4P did not change significantly with increased amount of inhibitor. The k_{cat} value decreased almost 50% when 10 mM inhibitor was present (Table 5). In Lineweaver-Burke plot, the error is significantly amplified at low substrate concentrations. Thus at 10 mM inhibitor, the last point was not considered when fitting the curve.

Surprisingly, both k_{cat} and K_M values for Mn^{2+} increased as a function of increased inhibitor's concentration (Table 6). It was unable to determine the kinetic parameters with 20 mM inhibitor, because the plateau region has not been reached with present data.

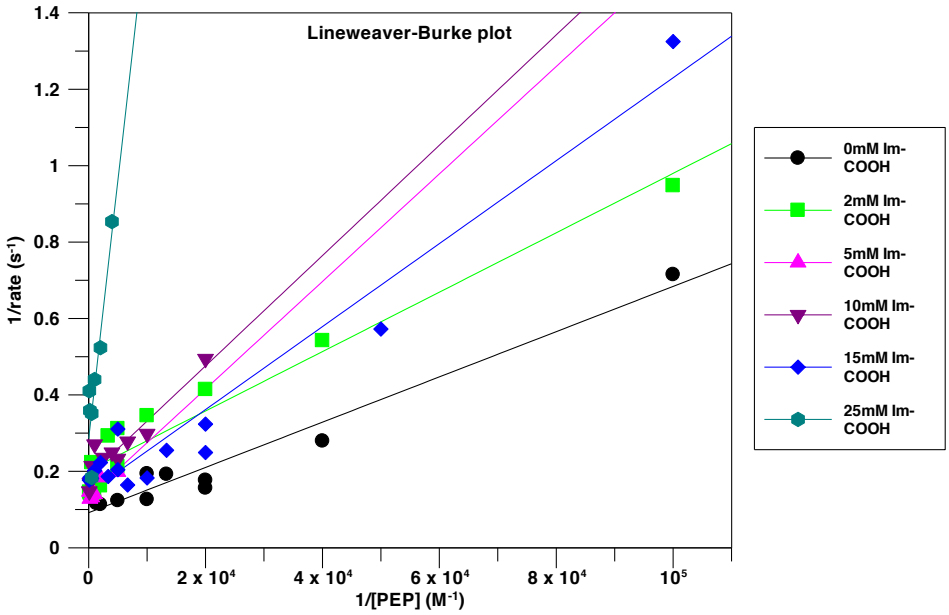

Figure 28. Inhibition type determination of 4-imidazolecarboxylic acid against PEP. The data is fitted into Lineweaver-Burke plot. (Im-COOH is known as 4-imidazolecarboxylic acid)

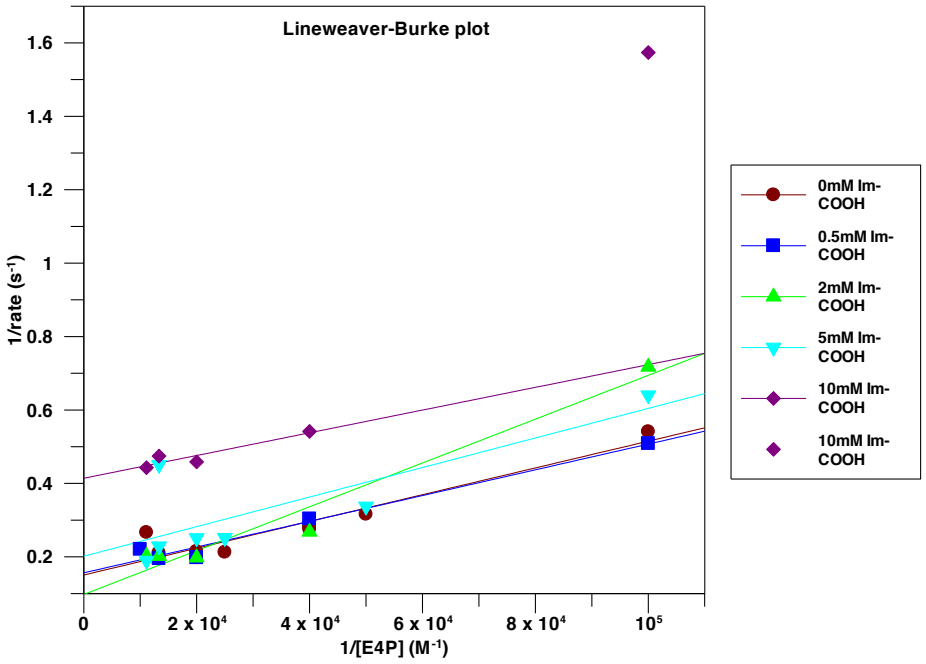

Figure 29. Inhibition type determination of 4-imidazolecarboxylic acid against E4P. The data is fitted into Lineweaver-Burke plot. (Im-COOH is known as 4-imidazolecarboxylic acid)

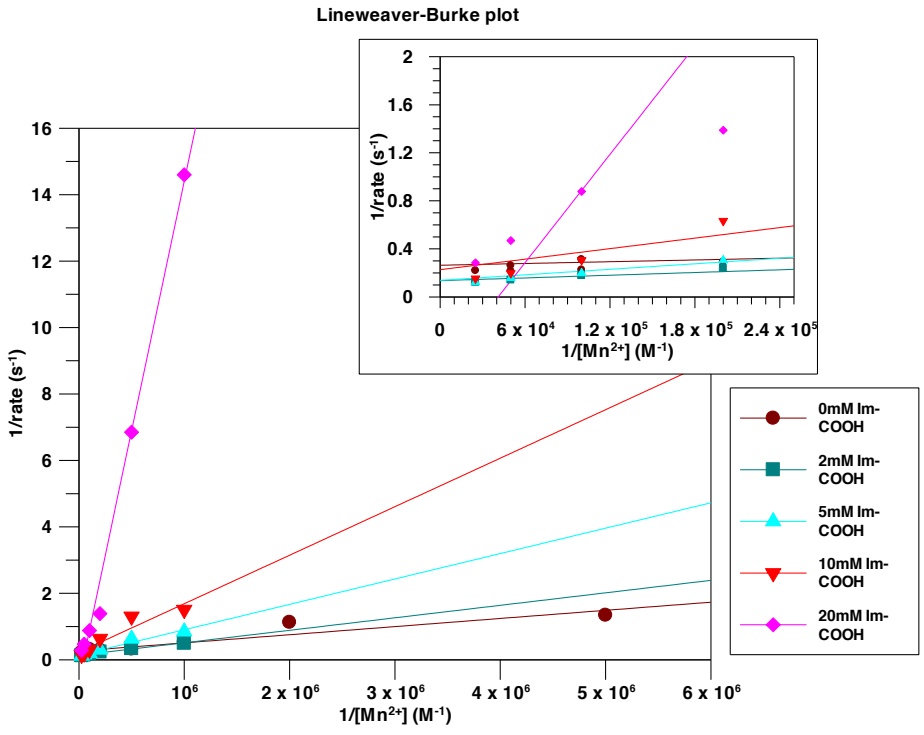

(A)

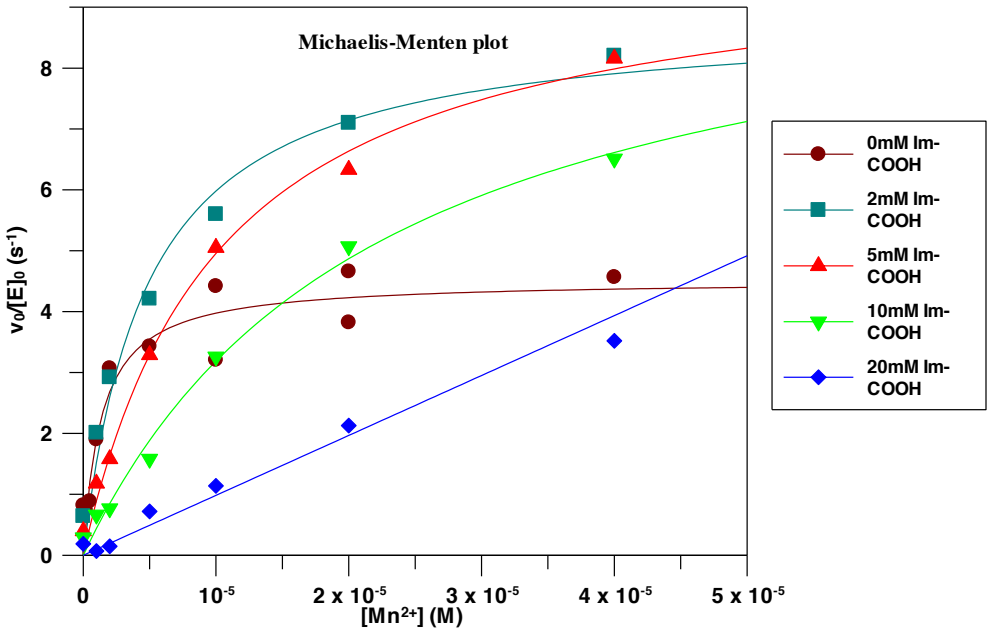

(B)

Figure 30. Inhibition type determination of 4-imidazolecarboxylic acid against Mn^{2+}. The data is fitted into both (A) Lineweaver-Burke plot and (B) Michaelis-Menten plot. (Im-COOH is known as 4-imidazolecarboxylic acid)

Table 4. Inhibition type determination of 4-imidazolecarboxylic acid against PEP. Summary of k_{cat} and K_M values obtained at different concentrations of inhibitor.

[4-imidazolecarboxylic acid] (mM)	k_{cat} (s^{-1})	K_M (M) (PEP)
0	8.9 ± 0.5	25.5 (± 9.1) × 10^{-6}
2	7.0 ± 0.2	18.7 (± 2.7) × 10^{-6}
5	7.6 ± 0.3	100 (± 37.5) × 10^{-6}
10	5.9 ± 0.3	96.4 (± 22.6) × 10^{-6}
15	5.8 ± 0.1	200 (± 8.2) × 10^{-6}
25	2.9 ± 0.2	300 (± 85.4) × 10^{-6}

Table 5. Inhibition type determination of 4-imidazolecarboxylic acid against E4P. Summary of k_{cat} and K_M values obtained at different concentrations of inhibitor.

[4-imidazolecarboxylic acid] (mM)	k_{cat} (s^{-1})	K_M (M) (E4P)
0	5.7 ± 0.5	14.4 (± 5.1) × 10^{-6}
0.5	6.0 ± 0.7	18.2 (± 7.2) × 10^{-6}
2	6.7 ± 0.8	24.1 (± 9.2) × 10^{-6}
5	5.0 ± 1.1	16.5 (± 13.8) × 10^{-6}
10	2.9 ± 0.4	20.3 (± 9.3) × 10^{-6}

Table 6. Inhibition type determination of 4-imidazolecarboxylic acid against Mn^{2+}. Summary of k_{cat} and K_M values obtained at different concentrations of inhibitor.

[4-imidazolecarboxylic acid] (mM)	k_{cat} (s^{-1})	K_M (M) (Mn^{2+})
0	4.5 ± 0.3	1.4 (± 0.4) × 10^{-6}
2	8.9 ± 0.6	4.8 (± 1.0) × 10^{-6}
5	10.0 ± 0.5	10.3 (± 1.4) × 10^{-6}
10	10.3 ± 0.9	22.3 (± 4.0) × 10^{-6}

Start codon determination

The long-form and short-form MurAs have a molecular weight discrepancy of 1905.3 Da. As illustrated in Figure 31, the genuine MurA band aligns with the long-form MurA standard, and both bands are slightly higher than short-form MurA standard. However, the difference is not yet sufficient enough to support such a conclusion.

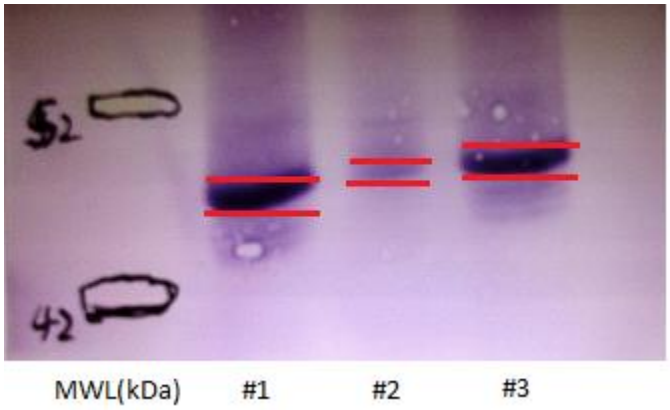

Figure 31. Western blot result for the determination of Bb_MurA's start codon. MWL=molecular weight ladder. (1) short-form Bb_MurA; (2) *Borrelia burgdorferi* cell pellet resuspension; (3) long-form Bb_MurA

Discussion

Bb_MurA purification and kinetic parameters characterization

MurA is a proven antimicrobial target, but only the Cys-containing enzymes are susceptible to fosfomycin. Tuberculosis, chlamydia, syphilis, and Lyme disease are all caused by bacteria that are naturally Asp-containing and therefore fosfomycin resistant. Developing new inhibitors against these enzymes requires that their activities be characterized in detail, but no natively Asp-containing MurA has previously been characterized. *C. trachomatis* MurA conferred fosfomycin resistance when expressed in *E. coli,* but could not be purified. *M. tuberculosis* MurA expressed in *E. coli* had no catalytic activity. Tuberculosis MurA was transiently expressed in *M. smegmatis*, but expression was unstable and eventually lost. The D117C mutant expressed in *M. smegmatis* rendered cell extracts fosfomycin-sensitive.

The inability of producing active natively Asp-containing MurA has always been the obstruction of antibacterial research, thus a yield of 10mg protein from 1L cell culture is considerable. The results indicate that the leaky expression of Bb_MurA during day-long incubation at 30°C in absence of IPTG is moderate enough to stop protein from forming aggregates or folding improperly, while yielding reasonable amount of protein.

The increased apparent activity upon overnight extended wash indicates that a non-covalent inhibitory ligand is co-purified with enzyme. UDP-MurNAc is a potential candidate of the inhibitor, which was previously co-purified with recombinant Ec_MurA.

At pH 7, Bb_MurA$_{H6}$ yields a k_{cat} = 0.74 s^{-1}, which is 6 times lower than Ec_MurA's, 3.8 s^{-1}, though pH 7 is close to Ec_MurA's optimal pH, while Bb_MurA's optimal pH was around pH 5. The long-form and short-form Bb_MurAs are equally active, making it impossible to determine the start codon of the natural enzyme kinetically. $K_{M,UDP\text{-}GlcNAc}$s are 56 µM and 24 µM respectively for short-form and long-form Bb_MurAs, which are similar to Ec_MurA's, 15 µM. $K_{M,PEP}$s were 66 µM and 39 µM, while the value for Ec_MurA is reported to be in the range of 0.2-4 µM. *B. burgdorferi* is reported to have an exponential phase generation time of 5 to 18 h in vivo, compared to 20 min for *E. coli*, so the k_{cat} of Bb_MurA we measured in vitro appears to be fast enough to support such a rate of cell growth. This result is also demonstrated that Asp115 in Bb_MurA is capable of fulfilling the two essential roles proposed for Cys115 in Ec_MurA, one as general acid/base catalyst and one involved in product release. Their positional similarity in the aligned sequences is consistent with this proposal.

In the Bb_MurA D116C mutant, the k_{cat} decreased by 20-fold. This is a fraction of MurA's overall catalytic enhancement, > 10^9-fold. Taking the previous data into consideration that the reciprocal mutation in Ec_MurA, C116D mutant's k_{cat} decreased modestly as well by 10-fold, we can establish that Asp and Cys are largely interchangeable in the active site of MurA.

The characterization of Bb_MurA shed light on the investigation of antibiotics which fight against multiple pathogens with Asp-containing MurAs. More importantly,

the elucidation of similar functionality between Cys 115 and Asp 116 indicates possibility of designing broad-spectrum inhibitors with efficacy against both types of MurA.

Fosfomycin titration

Cys-containing MurAs attack the epoxide functional group of fosfomycin, becoming alkylated and irreversibly inhibited. The kinetic mechanism for this inhibition reaction can be described by the following model:

Scheme 1.

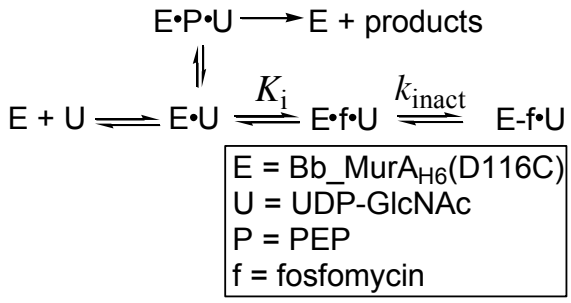

where fosfomycin initially forms a non-covalent complex with the UDP-GlcNAc bound enzyme, E•f•U, and then the covalent modification occurs, yielding E-f•U.

The value of k_{inact} was determined under conditions where [fosfomycin] >> K_i, so that [E•f•U] ≈ $[E]_{total}$. The first-order rate constant of inactivation, $k_{inact,}$ was fitted to be 0.021 ± 0.003 s^{-1}, comparing with 0.12 s^{-1} for Ec_MurA. The difference in reaction rates with fosfomycin is smaller than the difference in k_{cat} values (3.8 s^{-1} for Ec_MurA versus 0.03 s^{-1} for Bb_MurA D116C).

As fosfomycin occupies the same physical space in the MurA active site as PEP, it is a competitive inhibitor with respect to PEP. The dissociation equilibrium constant, K_i, was determined to be 5.7 ± 0.4 μM, compared with 8.6 μM for Ec_MurA.

Fosfomycin does not normally react with simple thiols, nor with most protein Cys residues. Under forcing conditions, it is eventually hydrolyzed to the diol, rather than being alkylated. The fast alkylation rate of the D116C mutant illustrated that C116 is not a typical non-enzymatic thiols, and that the active site environment of Bb_MurA D116C modifies its reactivity by increasing the Cys thiol's nucleophilicity and/or increasing the electrophilicity of the relatively inert epoxide functional group, like Ec_MurA. The reaction of Bb_MurA$_{H6}$ (D116C) with fosfomycin is also further evidence for functional similarity of the Asp116 and Cys115.

pH dependence

The maximum k_{cat} values for both long-form and short-form Bb_MurA$_{H6}$ in the pH profiles were achieved around pH 6, surprisingly low for an organism that is not known to have an unusual intracellular pH. The pK_{a1} values didn't change significantly from Bb_MurA$_{H6}$ to the D116C mutant, and were similar to the pK_a of an unperturbed carboxylate group. The dramatic shift in pK_{a2} in the D116C mutant demonstrated that pK_{a2} in the wild type enzyme, 7.4, is derived from the D116 side chain and that it must be protonated to be accounted for the fast catalytic turnover. The pK_a for an unperturbed Asp side chain is 4.0, 3.4 pH units lower than the determined pK_a in the

active site. pK_{a2} for the D116C mutant was >11, more than 2 pH units above the unperturbed pK_a of 8.3-9.1 for a Cys thiol. It appears that the active site environment of Bb_MurA is poised to perturb the pK_a of whatever residue is present at position 116, to bring catalytic amino acids into the appropriate protonation state at physiological pH.

Pyruvate oxime and glyoxylate oxime as inhibitors

Transition state structures are stabilized by the enzymes for the virtue of their geometric and electrostatic fit onto the transition-state conformation of the enzymes. For the TS mimics, the geometric similarities bring the molecules to the close proximity in the active site, and the electrostatic similarities participate in the formation of H-bond, hydrophobic contact, etc. Even though it is extremely challenging to achieve exact match, a reasonable binding affinity of the designed mimics indicates their similarities to the true transition-state structures, and their potential to be explored into potent inhibitors. The perfectly designed transition state mimics can bind to the enzyme 10^{10}-10^{15} times tighter than the substrates[40]. On the other hand, any slight discrepancy between the TS mimics and the geniune TS structures could potentially prevent the inhibitor from accessing the active site and hindering the catalysis.

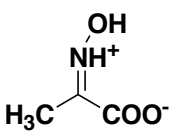

pyruvate oxime

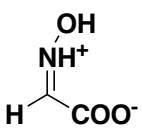

glyoxylate oxime

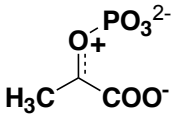

PEP cation

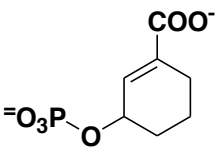

ddS3P

Pyruvate oxime was designed to mimic the structural and electrostatic features of the PEP cation. Glyoxylate oxime lacks a methyl group at C3 position, which creates more physical space in the active site for better interaction. However, neither of these molecules interacts with AroA/MurA effectively enough to inhibit the enzyme. The presence of ddS3P could potentially activate AroA through the binding of its remote phosphate and carboxylate groups, so that the oxacarbenium ion molecules can bind to the fitted structure of the enzyme optimally. This will require us to conquer the obstacle of synthesizing ddS3P, which has been attempted extensively but not yet succeeded. Otherwise, these two oxacarbenium ion molecules will have to be modified and altered fundamentally to simulate the TS structures in AroA/MurA catalysis and become effective inhibitors.

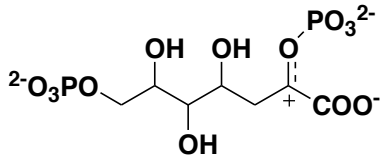

Oxacarbenium Ion Intermediate

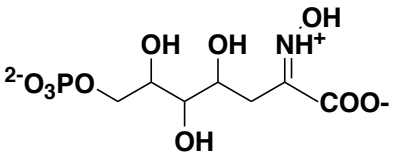

DAHP-oxime

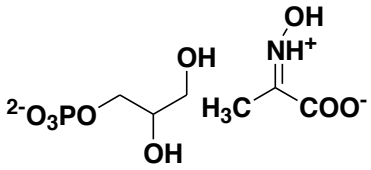

Glycerol 3-Phosphate Pyruvate Oxime

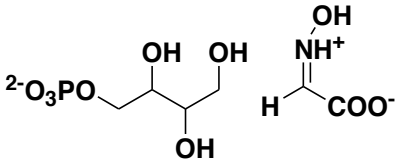

Glycerol Phosphate Glyoxylate Oxime

In comparison, pyruvate oxime and glyoxylate oxime exert similar inhibitory effect on DAHP synthase in the presence of glycerol 3-phosphate. The inhibition cannot be achieved by individual molecules but only with the combinatorial inhibitors. The essential role glycerol 3-phosphate plays could be contacting interactive amino acid residues on DAHP synthase, so as to introduce the conformational change of the enzyme to locate the TS mimics in the binding pockets. It is also possible that glycerol 3-phosphate and the TS mimics occupy the same physical space in the active site, and only

the presence of both molecules is capable of providing enough steric hindrance to substrate binding.

DAHP•oxime was previously designed to mimic the proposed transition-state structure and become positively charged on the atom at the same location. It has been determined to be a tight, slow binding inhibitor with a fitted equilibrium dissociation constant of 9×10^{-11} M[2 55]. Comparing to DAHP-oxime, the K_i value around 70 μM for pyruvate oxime and glyoxylate oxime is less satisfactory for the combinatorial inhibitors, but they still possess several great potentials for further optimization. First, the typical K_i range of inhibitors screened with fragment-based approach is 10 μM- mM, so it is reasonable to believe that our discovered combinatorial inhibitors could be modified into drug candidates whose K_i values are within 10 nM. Second, in fragment-based drug design, two molecular fragments are usually tethered together by a linker, so that the fragment that possesses better binding affinity towards the target could function as an anchor, locating the weaker binding fragment to adjacent binding pockets. In this way, the overall affinity of the linked compound is greatly enhanced. For our designed inhibitors, glycerol 3-phosphate and pyruvate oxime/glyoxylate oxime are un-tethered, but they can be modified individually, which cannot be accomplished with tethered compound. The scaffold of glycerol 3-phosphate could be substituted with less negatively charged moieties so as to pass the cell membrane more easily. The oxacarbenium ion molecules can be modified to involve greater proportion of atoms in the direct binding interaction. Third, the M.W. of the fragments is within 150 Da, which

is an essential feature for drug candidates, whose M.W. should be < 300 Da[39]. The mean M.W. of marketed oral drugs is 337 Da[50].

The similar K_i values obtained with pyruvate oxime and glyoxylic oxime indicate that the C3 methyl group is not required for binding and inhibition. By extension, from the exploration and comparison of a diversified oxacarbenium ion library, we will obtain more information regarding the functionality of different substituents, so as to design the optimum inhibitor for the target enzyme.

_R_-alanine, _L_-alanine, sulfamic acid and aminomethanesulfonic acid as inhibitors

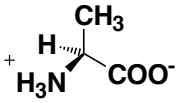

***S*-alanine**

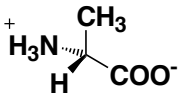

***R*-alanine**

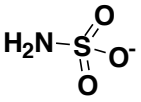

sulfamic acid

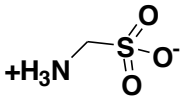

aminomethanesulfonic acid

Comparing to pyruvate oxime and glyoxylate oxime, the structure of alanine is more stable for its sp^3 hybridized C 2 atom, making it attractive template for the exploration of inhibitors. However, neither configuration of the alanines exerts inhibition towards DAHP synthase. The sulfate group in sulfamic acid and aminomethanesulfonic acid substitutes the carboxylate group in our previously investigated inhibitors. The length and main chain of the molecules are also altered, but no apparent inhibition was observed as a consequence of these modifications.

4-Imidazolecarboxylic acid as inhibitor

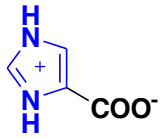

4-imidazolecarboxylic acid

4-Imidazolecarboxylic acid was evaluated as an inhibitor against DAHP synthase, and it appears to be a fast, tight binding inhibitor with fitted equilibrium dissociation constant of $3.0(\pm 0.2) \times 10^{-3}$ M.

The inhibition of 4-imidazolecarboxylic acid is positively cooperative, which indicates that the presence of one inhibitor molecule in its active site facilitates the binding of a second inhibitor molecule in other vacant active site. The kinetic data yields a well-fitted sigmoidal velocity curve (Figure 25). In the initial lag-phase, only minimal inhibition was achieved with increased amount of inhibitor. However, this binding introduces structural or electrostatic change on the enzyme, which increases the intrinsic binding affinity in other vacant active sites. The result is an inhibition profile in which inhibition is proportional to $[I]^2$. Similar cooperativity has been observed with DAHP•oxime, that two inhibitor molecules bind into the active sites of different subunits on DAHP synthase consecutively with progressive binding affinity. Various crystal structures of DAHP synthase have been obtained by Naresh Balachandran in the Berti lab, which provides further supporting evidence for cooperativity. DAHP synthase is a homotetramor. Once the first molecule of DAHP•oxime binds, the corresponding

subunit will exhibit a distinct conformation. Then the second inhibitor molecule enters the active site of the diagonal subunit, causing another unique set of conformational change. The remaining two subunits stay unoccupied, which presumably is responsible for the residual rate that has been observed in the presence of excess DAHP•oxime.

However, 4-imidazolecarboxylic acid also exhibits several distinct binding features comparing to DAHP•oxime. First, DAHP•oxime is a slow-binding inhibitor which requires certain interacting time to reach maximum inhibition. In contrast, the inhibition of 4-imidazolecarboxylic acid occurs instantly. Secondly, complete inhibition is achieved with 4-imizaolecarboxylic acid, compared to ~15% residual activity with excess DAHP•oxime. These features demonstrate that the binding pattern of 4-imidazolecarboxylic acid is distinct from DAHP•oxime, even though cooperativity is observed in both cases.

The inhibited rate decreased by 50% when 4 mM glycerol 3-phosphate was present (Figure 26), indicating that 4-imidazolecarboxylic acid inhibition is slightly improved by glycerol 3-phosphate. 4 mM glycerol 3-phosphate alone causes the activity of DAHP synthase decrease by 30%. This comparison suggests the possibility of cooperativity between the two molecules, but the difference is quite modest to support such conclusion. The K_i values and curves obtained with 4-imidazolecarboxylic acid alone and the combined inhibitors are essentially similar, so the binding type and functionality of the enzyme has not been altered by the addition of glycerol 3-phosphate.

If 4-imidazolecarboxylic acid binds to the DAHP•E4P•Mn^{2+} complex in the same physical space as PEP, then the inhibition is expected to be competitive with respect to PEP, and uncompetitive with respect to Mn^{2+} and E4P. The Lineweaver-Burke plot shows the expected pattern for competitive inhibition, with the lines intersecting at the Y-axis (Figure 28). The obtained K_M values of E4P are approximately 20 $\times 10^{-6}$ M under a variety of inhibitor concentration, and the decrease in k_{cat} values is observed when more than 5 mM inhibitor is utilized. These results support the uncompetitive binding pattern of 4-imidazolecarboxylic acid with respect to E4P. The characterization regarding Mn^{2+} is ambiguous, as both k_{cat} and K_M increase. To explore the definitive binding pocket of 4-imidaozlecarboxylic acid, crystallography attempts will be required, where DAHP synthase is co-crystallized with the inhibitor.

DAHP synthase catalysis follows a terreactant mechanism, where Mn^{2+}, E4P and PEP are considered to bind consecutively after each other. The configuration of the enzyme provides four potential active sites, even though only two of them are assumed to be responsible for the substrates turnover. 4-imidazolecarboyxlic acid molecules are also preliminarily determined to bind to the enzyme following a sequential order. All these factors contribute to the complexity in the inhibition of 4-imidazolecarboxylic acid towards DAHP synthase. To simplify the binding event, we assume that substrate binding is not cooperative, but the inhibitor binding has strong positive cooperativity. So in the fitting equation, only the item representing DAHPS•Mn^{2+}•E4P complex is multiplied by the factor of $[I]^2/K_i^2$. The determined K_i for 4-imidazolecarboxylic is around

2×10^{-3} M, but this number does not correspond to weaker potency. From Figure 24B, we can observe that the IC_{50} of 4-imidazolecarboxylic acid is less than 10 mM. In contrast, it takes more than 20 mM pyruvate oxime or glyoxylate oxime to reach 50% inhibition, even their K_i values are approximately 70 μM.

For molecules that are potent for their size, the concept of Ligand Efficiency (LE) has been used to assess their potency and potential as drug leads. LE is defined as:

$$\mathrm{LE} = {-\Delta G}/{\mathrm{HAC}} = {-\mathrm{RT}\ln(K_i)}/{\mathrm{HAC}} \quad ,$$

where HAC represents the number of heavy atoms in the molecule[50,51]. For strong-binding inhibitor, the average binding free energy for each non-hydrogen atom is approximately 1.5 kcal/mol[50]. Compounds that possess LE of 0.3 or better generally obey the Lipinski rules and are considered as reasonable drug candidates[50]. 4-Imidazolecarboxylic acid's K_i is ~ 3mM, and it contains 8 heavy atoms. Its calculated LE is 0.29, which is further evidence for its potency, and its potential to be modified into a 10 nM range inhibitor.

In 2009, Walker's group published their investigation on inhibitor design of DAHP synthase, where a variety of substrate and reaction intermediate mimics were synthesized and evaluated[52]. They concluded that the molecules whose carboxylate and phosphonate/phosphate groups are separated by a distance similar to those in PEP are effective competitive inhibitors with respect to PEP. The most potent inhibitor they

discovered was the vinyl phosphonate, (E)-2-methyl-3-phosphonoacrylic acid, with a K_i of 4.7 μM. Recently, they modified these PEP-site parental molecules with a well-positioned phosphate moiety, allowing the molecule to enter the binding sites of both substrates simultaneously[53]. Slight increase in binding affinity and potency were observed with the extended inhibitors.

The inhibitors introduced above are all derived from the scaffold of the substrates and intermediates in the catalysis. However, 4-imidazolecarboxylic acid exhibits no structural similarity to either substrate, indicating the possibility of a distinct binding pattern. Imidazole alone has no inhibition effect on the enzyme, which lends further support to the hypothesis that the TS structures in DAHP synthase's catalysis are oxacarbenium ion molecules. In the future, we can alter the scaffold of 4-imidazolecarboxylic acid by substituting the N atom in the imidazole ring with its hetero atoms, or locating the carboxylic acid group at different location on the ring. Starting with fragments as efficient as 4-imidazolecarboxylic acid is likely to achieve reasonably sized, potent molecules as drug candidates.

Conclusion and Future work

To explore the catalytic mechanism of MurA from *Borrelia burgdorferi*, His-tagged Bb_MurA and its D116C mutant have been successfully expressed, purified and characterized. Asp116 in Bb_MurA has been demonstrated to be capable of fulfilling the two essential roles proposed for Cys115 in Ec_MurA, one as general acid/base catalyst and one involved in product release. The fast alkylation rate of fosfomycin to the D116C mutant illustrated that C116 is not a typical non-enzymatic thiols, and that the active site environment of Bb_MurA D116C is essentially similar to Ec_MurA.

Several mechanism-based inhibitors, including pyruvate oxime, glyoxylate oxime and 4-imidazolecarboxylic acid, have been discovered and evaluated as inhibitors of DAHP synthase. Pyruvate oxime/glyoxylate oxime's inhibition can only occur in the presence of glycerol 3-phosphate. 4-Imidazolecarboxylic acid's inhibition is discovered to be cooperative, and its binding is competitive with respect to PEP, and uncompetitive with respect to E4P.

Crystallography, kinetic isotope effect (KIE) analysis, HTS and other biological methods will be required for the exploration of better inhibitors for MurA and AroA. It will also be of paramount importance to explore a diversified oxacarbenium ion library, so as to involve greatest proportion of atoms on the inhibitor directly into the binding interaction. It is reasonable to anticipate that the continuous application and

optimization will help us discover powerful transition state inhibitors, and ultimately they will be incorporated with desired pharmacologic properties.

References

(1) Stanley, S. A.; Hung, D. T. Chemical Tools for Dissecting Bacterial Physiology and Virulence. *Biochemistry* **2009***, 48*, 8776-8786.

(2) Wolfenden, R.; Snider, M. J. The Depth of Chemical Time and the Power of Enzymes as Catalysts. *Acc. Chem. Res.* **2001***, 34*, 938-945.

(3) Robertson, J. G. Mechanistic Basis of Enzyme-Targeted Drugs. *Biochemistry* **2005***, 44*, 5561-5571.

(4) Baum, E. Z.; Montenegro, D. A.; Licata, L.; Turchi, I.; Webb, G. C.; Foleno, B. D.; Bush, K. Identification and Characterization of New Inhibitors of the Escherichia coli MurA Enzyme. *Antimicrob. Agents Chemother.* **2001***, 45*, 3182-3188.

(5) Coggins, J. R.; Abell, C.; Evans, L. B.; Frederickson, M.; Robinson, D. A.; Roszak, A. W.; Lapthorn, A. P. Experiences with the shikimate-pathway enzymes as targets for rational drug design. *Biochem. Soc. Trans.* **2003***, 31*, 548-552.

(6) Jackson, S. G.; Zhang, F.; Chindemi, P.; Junop, M. S.; Berti, P. J. Evidence of Kinetic Control of Ligand Binding and Staged Product Release in MurA (Enolpyruvyl UDP-GlcNAc Synthase)-Catalyzed Reactions, *Biochemistry* **2009***, 48*, 11715-11723.

(7) Berti, P. J.; Chindemi, P. Catalytic Residues and an Electrostatic Sandwich That Promote Enolpyruvyl Shikimate 3-Phosphate Synthase (AroA) Catalysis. *Biochemistry* **2009***, 48*, 3699-3707.

(8) El, Z., Ahmed; Sanschagrin, F.; Levesque, R. C. Structure and function of the Mur enzymes: development of novel inhibitors. *Mol. Microbiol.* **2003***, 47*, 1-12.

(9) Skarzynski, T.; Mistry, A.; Wonacott, A.; Hutchinson, S. E.; Kelly, V. A.; Duncan, K. Structure of UDP-N-acetylglucosamine enolpyruvyl transferase, an enzyme essential for the synthesis of bacterial peptidoglycan, complexed with substrate UDP-N-acetylglucosamine and the drug fosfomycin. *Structure* **1996***, 4*, 1465-1474.

(10) Schönbrunn, E.; Sack, S.; Eschenburg, S.; Perrakis, A.; Krekel, F.; Amrhein, N.; Mandelkow, E. Crystal structure of UDP-N-acetylglucosamine enolpyruvyltransferase, the target of the antibiotic fosfomycin. *Structure* **1996***, 4*, 1065-1075.

(11) Anderson, K. S.; Johnson, K. A. "Kinetic competence" of the 5-enolpyruvoylshikimate-3-phosphate synthase tetrahedral intermediate. *J. of Biol. Chem.* **1990***, 265*, 5567-5572.

(12) Eschenburg, S.; Kabsch, W.; Healy, M. L.; Schönbrunn, E. A New View of the Mechanisms of UDP-N-Acetylglucosamine Enolpyruvyl Transferase (MurA) and 5-Enolpyruvylshikimate-3-phosphate Synthase (AroA) Derived from X-ray Structures of Their Tetrahedral Reaction Intermediate States. *J. of Biol. Chem.* **2003***, 278*, 49215-49222.

(13) Funke, T.; Yang, Y.; Han, H.; Healy-Fried, M.; Olesen, S.; Becker, A.; Schönbrunn, E. Structural Basis of Glyphosate Resistance Resulting from the Double Mutation Thr97 → Ile and Pro101 → Ser in 5-Enolpyruvylshikimate-3-phosphate Synthase from Escherichia coli. *J. of Biol. Chem.* **2009***, 284*, 9854-9860.

(14) Anderson, K. S.; Sikorski, J. A.; Benesi, A. J.; Johnson, K. A. Isolation and structural elucidation of the tetrahedral intermediate in the EPSP synthase enzymic pathway. *J. Am. Chem. Soc.* **1988***, 110*, 6577-6579.

(15) Anderson, K. S.; Sikorski, J. A.; Johnson, K. A. Evaluation of 5-enolpyruvoylshikimate-3-phosphate synthase substrate and inhibitor binding by stopped-flow and equilibrium fluorescence measurements. *Biochemistry* **1988***, 27*, 1604-1610.

(16) Gruys, K. J.; Walker, M. C.; Sikorski, J. A. Substrate synergism and the steady-state kinetic reaction mechanism for EPSP synthase from Escherichia coli. *Biochemistry* **1992***, 31*, 5534-5544.

(17) Zhang, F.; Berti, P. J. Phosphate Analogues as Probes of the Catalytic Mechanisms of MurA and AroA, Two Carboxyvinyl Transferasesâ€. *Biochemistry* **2006***, 45*, 6027-6037.

(18) Walsh, C. T.; Benson, T. E.; Kim, D. H.; Lees, W. J. The versatility of phosphoenolpyruvate and its vinyl ether products in biosynthesis. *Chem. Biol.* **1996***, 3*, 83-91.

(19) Byczynski, B.; Mizyed, S.; Berti, P. J. Nonenzymatic Breakdown of the Tetrahedral Intermediates of MurA and AroA, Two Carboxyvinyl Transferases. Protonation of Different Functional Groups Controls the Rate and Fate of Breakdown. *J. Am. Chem. Soc.* **2003***, 125*, 12541-12550.

(20) Kim, D. H.; Lees, W. J.; Kempsell, K. E.; Lane, W. S.; Duncan, K.; Walsh, C. T. Characterization of a Cys115 to Asp Substitution in the Escherichia coli Cell Wall

Biosynthetic Enzyme UDP-GlcNAc Enolpyruvyl Transferase (MurA) That Confers Resistance to Inactivation by the Antibiotic Fosfomycinâ€. *Biochemistry* **1996***, 35*, 4923-4928.

(21) Schonbrunn, E.; Eschenburg, S.; Krekel, F.; Luger, K.; Amrhein, N. Role of the Loop Containing Residue 115 in the Induced-Fit Mechanism of the Bacterial Cell Wall Biosynthetic Enzyme MurA. *Biochemistry* **2000***, 39*, 2164-2173.

(22) Isaacs, R. D. Borrelia burgdorferi bind to epithelial cell proteoglycans. *J. Clin. Invest.* **1994***, 93*, 809-19.

(23) Mizyed, S.; Oddone, A.; Byczynski, B.; Hughes, D. W.; Berti, P. J. UDP-N-acetylmuramic Acid (UDP-MurNAc) Is a Potent Inhibitor of MurA (Enolpyruvyl-UDP-GlcNAc Synthase). *Biochemistry* **2005***, 44*, 4011-4017.

(24) Han, H.; Yang, Y.; Olesen, S. H.; Becker, A.; Betzi, S.; Schonbrunn, E. The Fungal Product Terreic Acid Is a Covalent Inhibitor of the Bacterial Cell Wall Biosynthetic Enzyme UDP-N-Acetylglucosamine 1-Carboxyvinyltransferase (MurA), *Biochemistry* **2010***, 49*, 4276-4282.

(25) Rausch, S.; Hanchen, A.; Denisiuk, A.; Lahken, M.; Schneider, T.; Sassmuth, R. D. Feglymycin is an Inhibitor of the Enzymes MurA and MurC of the Peptidoglycan Biosynthesis Pathway. *ChemBioChem* **2011***, 12*, 1171-1173.

(26) Anton, D. L.; Hedstrom, L.; Fish, S. M.; Abeles, R. H. Mechanism of enolpyruvylshikimate-3-phosphate synthase exchange of phosphoenolpyruvate with solvent protons. *Biochemistry* **1983***, 22*, 5903-5908.

(27) Boocock, M. R.; Coggins, J. R. Kinetics of 5-enolpyruvylshikimate-3-phosphate synthase inhibition by glyphosate. *FEBS Lett.* **1983***, 154*, 127-133.

(28) Sammons, R. D.; Gruys, K. J.; Anderson, K. S.; Johnson, K. A.; Sikorski, J. A. Reevaluating Glyphosate as a Transition-State Inhibitor of EPSP Synthase: Identification of an EPSP Synthase.EPSP.Glyphosate Ternary Complex. *Biochemistry* **1995***, 34*, 6433-6440.

(29) Sikorski, J. A.; Gruys, K. J. Understanding Glyphosate's Molecular Mode of Action with EPSP Synthase: Evidence Favoring an Allosteric Inhibitor Model. *Acc. Chem. Res.* **1997***, 30*, 2-8.

(30) Kim, D. H.; Tucker-Kellogg, G.; Lees, W. J.; Walsh, C. T. Analysis of Fluoromethyl Group Chirality Establishes a Common Stereochemical Course for the Enolpyruvyl

Transfers Catalyzed by EPSP Synthase and UDP-GlcNAc Enolpyruvyl Transferase. *Biochemistry* **1996***, 35*, 5435-5440.

(31) Alberg, D. G.; Lauhon, C. T.; Nyfeler, R.; Faessler, A.; Bartlett, P. A. Inhibition of 5-enolpyruvoylshikimate 3-phosphate (EPSP) synthase by analogs of the tetrahedral intermediate and of EPSP. *J. Am. Chem. Soc.* **1992***, 114*, 3535-3546.

(32) Eschenburg, S.; Priestman, M.; Schönbrunn, E. Evidence That the Fosfomycin Target Cys115 in UDP-N-acetylglucosamine Enolpyruvyl Transferase (MurA) Is Essential for Product Release. *J. of Biol. Chem.* **2005***, 280*, 3757-3763.

(33) Krekel, F.; Samland, A. K.; Macheroux, P.; Amrhein, N.; Evans, J. N. S. Determination of the pKa Value of C115 in MurA (UDP-N-Acetylglucosamine Enolpyruvyltransferase) from Enterobacter cloacae. *Biochemistry* **2000***, 39*, 12671-12677.

(34) Mizyed, S.; Wright, J. E. I.; Byczynski, B.; Berti, P. J. Identification of the Catalytic Residues of AroA (Enolpyruvylshikimate 3-Phosphate Synthase) Using Partitioning Analysisâ€ . *Biochemistry* **2003***, 42*, 6986-6995.

(35) White, R. E. High-Throughput Screening in Drug Metabolism and Pharmacokinetic Support of Drug Discovery. *Annu. Rev. Pharmacol. Toxicol.* **2000***, 40*, 133-157.

(36) Hertzberg, R. P.; Pope, A. J. High-throughput screening: new technology for the 21st century. *Curr. Opin. Chem. Biol.* **2000***, 4*, 445-451.

(37) Bajorath, J. Integration of virtual and high-throughput screening. *Nat Rev Drug Discov* **2002***, 1*, 882-894.

(38) Jencks, W. P. On the attribution and additivity of binding energies. *Proceedings of the National Academy of Sciences* **1981***, 78*, 4046-4050.

(39) Rees, D. C.; Congreve, , Miles; Murray, C. W.; Carr, R. Fragment-based lead discovery. *Nat Rev Drug Discov* **2004***, 3*, 660-672.

(40) Schramm, V. L. Enzymatic Transition States and Transition State Analog Design. *Annu. Rev. Biochem.* **1998***, 67*, 693-720.

(41) Clark, M. E.; Berti, P. J. Enolpyruvyl Activation by Enolpyruvylshikimate-3-phosphate Synthase. *Biochemistry* **2007***, 46*, 1933-1940.

(42) DeLeo, A. B.; Dayan, J.; Sprinson, D. B. Purification and Kinetics of Tyrosine-sensitive 3-Deoxy-d-arabino-heptulosonic Acid 7-Phosphate Synthetase from Salmonella. *J. Biol. Chem.* **1973***, 248*, 2344-2353.

(43) Floss, H. G.; Onderka, D. K.; Carroll, M. Stereochemistry of the 3-Deoxy-d-arabino-heptulosonate 7-Phosphate Synthetase Reaction and the Chorismate Synthetase Reaction. *J. Biol. Chem.* **1972***, 247*, 736-744.

(44) Hedstrom, L.; Abeles, R. 3-Deoxy-D-manno-octulosonate-8-phosphate synthase catalyzes the C-O bond cleavage of phosphoenolpyruvate. *Biochem. Biophys. Res. Commun.* **1988***, 157*, 816-820.

(45) Shumilin, I. A.; Bauerle, R.; Wu, J.; Woodard, R. W.; Kretsinger, R. H. Crystal Structure of the Reaction Complex of 3-Deoxy-d-arabino-heptulosonate-7-phosphate Synthase from Thermotoga maritima Refines the Catalytic Mechanism and Indicates a New Mechanism of Allosteric Regulation. *J. Mol. Biol.* **2004***, 341*, 455-466.

(46) Herrmann, K. M.; Weaver, L. M. The Shikimate Pathway. *Annu. Rev. Plant Physiol. Plant Mol. Biol.* **1999***, 50*, 473-503.

(47) Li, Z.; Sau, A. K.; Shen, S.; Whitehouse, C.; Baasov, T.; Anderson, K. S. A Snapshot of Enzyme Catalysis Using Electrospray Ionization Mass Spectrometry. *J. Am. Chem. Soc.* **2003***, 125*, 9938-9939.

(48) Pace, C. N.; Vajdos, F.; Fee, L.; Grimsley, G.; Gray, T. How to measure and predict the molar absorption coefficient of a protein. *Protein Science* **1995***, 4*, 2411-2423.

(49) Schoner, R.; Herrmann, K. M. 3-Deoxy-D-arabino-heptulosonate 7-phosphate synthase. Purification, properties, and kinetics of the tyrosine-sensitive isoenzyme from Escherichia coli. *J. Biol. Chem.* **1976***, 251*, 5440-5447.

(50) Carr, R. A. E.; Congreve, M.; Murray, C. W.; Rees, D. C. Fragment-based lead discovery: leads by design. *Drug Discov. Today* **2005***, 10*, 987-992.

(51) Hopkins, A. L.; Groom, C. R.; Alex, A. Ligand efficiency: a useful metric for lead selection. *Drug Discov. Today* **2004***, 9*, 430-431.

(52) Walker, S. R.; Cumming, H.; Parker, E. J. Substrate and reaction intermediate mimics as inhibitors of 3-deoxy-d-arabino-heptulosonate 7-phosphate synthase. *Org. Biomol. Chem.* **2009***, 7*, 3031-3035.

(53) Walker, S. R.; Jiao, W.; Parker, E. J. Synthesis and evaluation of dual site inhibitors of 3-deoxy-d-arabino-heptulosonate 7-phosphate synthase. *Bioorg. Med. Chem. Lett. , In Press, Corrected Proof*.

(54) An, M.; Maitra, U.; Neidlein, U.; Bartlett, P. A. 5-Enolpyruvylshikimate 3-Phosphate Synthase: Chemical Synthesis of the Tetrahedral Intermediate and Assignment of the Stereochemical Course of the Enzymatic Reaction. *J. Am. Chem. Soc.* **2003***, 125*, 12759-12767.

(55) Balachandran, N.; Berti, P. Unpublished data.